The Canadian Mineralogist
Vol. 49, pp. 721-747 (2011)
DOI: 10.3749/canmin.49.3.721

REGIONAL LOW-PRESSURE AMPHIBOLITE-FACIES METAMORPHISM AT THE PIPE II MINE, THOMPSON NICKEL BELT, MANITOBA, AND COMPARISON OF METAMORPHIC ISOGRADS IN METAPELITES AND META-IRON FORMATIONS

Chris G. COUËSLAN[§] and David R.M. PATTISON

Department of Geoscience, University of Calgary, Calgary, Alberta T2N 1N4, Canada

Douglas K. TINKHAM

Department of Earth Sciences, Laurentian University, Sudbury, Ontario P3E 2C6, Canada

Abstract

The Ospwagan Group supracrustal sequence of the Thompson Nickel Belt, Manitoba, includes semipelitic and pelitic schist, iron formation, and mafic volcanic rocks that were deformed and metamorphosed during the Trans-Hudson orogeny (*ca.* 1.8 Ga). North–south-trending metamorphic isograds at the Pipe II mine in the central portion of the belt show the following sequence from west to east: (1) andalusite + staurolite-out, in metapelites, (2) orthopyroxene-in, in meta-iron formations, (3) sillimanite + K-feldspar-in, in metapelites and semipelites. A roughly NE–SW-trending migmatite-in isograd (4), in semipelites, transects isograd (3) in the south portion of the study area. Equilibrium-assemblage diagrams for representative bulk-compositions were calculated using the Theriak–Domino software to provide pressure and temperature constraints for each of the metamorphic isograds. Isograds developed at the following metamorphic conditions: isograd (1) 585–600°C, 3.7–3.9 kbar, isograd (2) 625–640°C, 3.0–3.9 kbar, and isograd (3) 640–660°C at 3.0–3.6 kbar. The position of isograd (2), orthopyroxene-in for iron formation, occurs down-grade of isograd (3), sillimanite + K-feldspar-in for pelites, roughly 125°C below temperatures of granulite-facies metamorphism. The appearance of orthopyroxene at the middle amphibolite-facies to upper-amphibolite-facies transition is favored by the Fe- and Mn-rich bulk composition of the iron formation. The oblique orientation of isograd (4) to isograds (1–3) may be the result of an increasing pressure gradient toward the south, or the infiltration of melt-inducing fluids, or both. The isograd sequence suggests an apparent thermal gradient of at least 65°C over 420 m. The metastable persistence of staurolite and andalusite could result in an actual gradient closer to 30°C.

Keywords: low-pressure regional metamorphism, iron formation, orthopyroxene, pelite, Thompson Nickel Belt, Manitoba.

Sommaire

La séquence supracrustale du Groupe d'Ospwagan, dans la ceinture nickelifère de Thompson, comprend des schistes semipélitiques et pélitiques, des formations de fer, et des roches volcaniques mafiques déformées et métamorphisées lors de l'orogenèse Trans-Hudson (*ca.* 1.8 Ga). Les isogrades métamorphiques à la mine Pipe II, dans la partie centrale de cette ceinture, alignés nord–sud, montrent la séquence suivante allant de l'ouest vers l'est: (1) déstabilisation de andalusite + staurolite, dans les métapélites, (2) apparition de l'orthopyroxène, dans les formations de fer métamorphisées, (3) apparition de sillimanite + feldspath potassique, dans les métapélites et semipélites. Un isograde aligné NE–SO marque l'apparition de la migmatite (4), dans les semipélites, recoupe l'isograde (3) dans la portion sud de la région étudiée. Les diagrammes montrant les assemblages à l'équilibre pour des compositions globales représentatives ont été calculés au moyen du logiciel Theriak–Domino afin de mieux délimiter la pression et la température pour chaque isograde. Les isogrades se sont développés aux conditions métamorphiques suivantes: isograde (1): 585–600°C, 3.7–3.9 kbar, isograde (2): 625–640°C, 3.0–3.9 kbar, et isograde (3): 640–660°C at 3.0–3.6 kbar. La position de l'isograde (2), marquant l'apparition de l'orthopyroxène dans les formations de fer, est située en dessous de l'isograde (3), sillimanite + feldspath potassique dans les pélites, et environ 125°C plus bas que le seuil d'un métamorphisme au faciès granulite. L'apparition de l'orthopyroxène aux conditions transitionnelles du faciès amphibolite moyen à amphibolite supérieur serait favorisée par la composition riche en Fe et en Mn des formations de fer. L'orientation oblique de l'isograde (4)

[§] *E-mail address*: chris.coueslan@gov.mb.ca. *Present address*: Manitoba Geological Survey, Manitoba Innovation, Energy, and Mines, Winnipeg, Manitoba R3G 3P2, Canada

par rapport aux isogrades (1–3) pourrait résulter d'un gradient de pression augmentant vers le sud, ou bien de l'infiltration de fluides provoquant l'anatexie, ou les deux. La séquence des isogrades serait conforme à un gradient thermique d'au moins 65°C étalé sur 420 m. La persistance métastable de la staurolite et de l'andalusite pourrait imposer un gradient plus près de 30°C.

(Traduit par la Rédaction)

Mots-clés: métamorphisme régional à faible pression, formation de fer, orthopyroxène, pélite, ceinture nickelifère de Thompson, Manitoba.

INTRODUCTION

The Thompson Nickel Belt forms a segment of the Superior Boundary Zone of Manitoba (Fig. 1; Bell 1971, Bleeker 1990a). The Superior Boundary Zone represents the margin of the Superior craton that was tectonically reworked by the collision of the Hearne craton and accreted Paleoproterozoic arc-derived terranes during the Trans-Hudson orogeny (Bleeker 1990a, Weber 1990, Ansdell 2005). The 030°-trending Thompson Nickel Belt has a width of 10 to 35 km and a strike length of almost 400 km; however, the southern third to half of the belt is covered by Paleozoic limestone (Burnham *et al.* 2009). Although the Thompson Nickel Belt has been the subject of structural, lithological, geochemical, geochronological, and tectonic studies over the last two decades (Fueten & Robin 1989, Bleeker 1990a, 1990b, Ansdell 2005, Gapais *et al.* 2005, Zwanzig *et al.* 2007, Burnham *et al.* 2009), few investigators have examined the metamorphic history of the belt.

This study is part of a regional investigation of the Hudsonian metamorphism of the Thompson Nickel Belt (Couëslan *et al.* 2007). The Pipe II mine is considered an ideal starting point because of its central location within the Thompson Nickel Belt, extensive exposures of a variety of lithologies, and the presence of a previously recognized, though not precisely located, muscovite-out metamorphic isograd (Bleeker 1990a). The varied lithologies at this site include both silicate-facies iron formations and pelitic schists. Iron formations are relatively widespread in Precambrian sequences around the world (Klein 2005), and can contain low-variance mineral assemblages useful in estimating metamorphic conditions. The Pipe II mine is therefore a good location to test the ability of current thermodynamic databases to model the low-Mg# bulk compositions of iron formations and compare this to the better-tested thermodynamic datasets for pelitic bulk-compositions.

Although the metamorphism of the Pipe II mine area has been addressed as part of previous regional studies (Fueten *et al.* 1986, Fueten & Robin 1989, Bleeker 1990a, 1990b, Burnham *et al.* 2009), a dedicated metamorphic study has not been published. The first part of the paper consists of a detailed petrographic description and interpretation of the metamorphic assemblages, and the identification of metamorphic isograds. In the second part of the paper, thermodynamic modeling is used to quantify the pressure–temperature conditions and the range in metamorphic grade represented by the mineral assemblages. This includes a comparison between metamorphic assemblages in metapelites and meta-iron formations.

GENERAL GEOLOGY

Prior to the Trans-Hudson orogeny, Paleoproterozoic supracrustal rocks of the Ospwagan Group were unconformably deposited on exhumed Archean gneisses of the Superior craton (Scoates *et al.* 1977, Bleeker 1990a, Zwanzig *et al.* 2007). The metasedimentary sequence of the Ospwagan Group consists of a fining upward siliciclastic sequence (the Manasan Formation), grading into calcareous metasediments of the Thompson Formation. The calcareous metasediments are overlain by deeper-basin siliciclastic and chemical metasediments of the Pipe Formation, which grade into the Setting Formation, a coarsening-upward package of siliciclastic rocks. The Setting Formation is finally capped by a thick sequence of mafic to ultramafic metavolcanic rocks of the Bah Lake Assemblage (Bleeker 1990a, Zwanzig *et al.* 2007). Although rocks of the Ospwagan Group are derived largely from detritus of Archean age originating from the Superior craton (Burnham *et al.* 2009), Paleoproterozoic detrital zircon has been extracted from Manasan and Setting formations, yielding maximum ages of deposition of 2235 ± 45 and 1974 ± 50 Ma, respectively (Bleeker & Hamilton 2001, Burnham *et al.* 2009). A further constraint on the age is provided by mafic dykes of Molson age and the nickel ore-bearing ultramafic sills that intruded the Ospwagan Group supracrustal rocks at all stratigraphic levels at *ca.* 1880 Ma (Bleeker 1990a, Burnham *et al.* 2009, Heaman *et al.* 2009).

Deformation during the Trans-Hudson orogeny is interpreted to have occurred in four main events, all affecting the Ospwagan Group. The F_1 event predates the intrusion of the *ca.* 1880 Ma mafic dykes, and has been interpreted as a nappe-forming event (Bleeker 1990a), or a relatively open, upright folding event (Burnham *et al.* 2009). The F_1 folds can only be observed where suitable markers are present, and the resulting deformation is poorly defined. The second deformation event, D_2, caused refolding and tightening of the F_1 folds and resulted in southwest-verging, isoclinal to recumbent F_2 folds (Burnham *et al.* 2009).

Previous workers considered this event coincident with peak conditions of metamorphism of the lower amphibolite to granulite facies in the Thompson Nickel Belt, as made evident by the regionally penetrative S_2 and L_2 fabrics and the isoclinal to recumbent nature of the regional ductile folding (Bleeker 1990a, Burnham *et al.* 2009). The main regional foliation (S_2) is subparallel to S_0 layering of Ospwagan Group rocks and the Archean gneissosity (Paktunç & Baer 1986, Bleeker 1990a, Zwanzig *et al.* 2007, Burnham *et al.* 2009). The D_2 event was likely related to the collision of the Superior craton with the allochthonous Kisseynew Domain of the Trans-Hudson Orogen at *ca.* 1840–1800 Ma (Ansdell 2005, Burnham *et al.* 2009). Local strain-free porphyroblasts and quartz–sillimanite knots flattened in S_3 suggest that peak conditions of metamorphism outlasted D_2 and were maintained into D_3 (*ca.* 1770 to 1760 Ma, Bleeker 1990a, Zwanzig 1998, Burnham *et al.* 2009). Tight, isoclinal F_3 folds with vertical to steeply southeast-dipping axial planes are the dominant fold structures in the Thompson Nickel Belt. Infolded Archean gneiss and Ospwagan Group rocks typically form elongate chains of northeast-trending, doubly plunging F_3 synforms and antiforms (Bleeker 1990a, Burnham *et al.* 2009). The D_3 deformation event is attributed to northwest–southeast shortening and regional, southeast-side-up, sinistral transpression (Bleeker 1990a, Burnham *et al.* 2009). Tightening of F_2–F_3 structures continued during D_4, which was accompanied by localized retrograde greenschist-facies metamorphism along mylonitic and brittle cataclastic shear zones commonly indicating a southeast-side-up sinistral movement (Bleeker 1990a, Burnham *et al.* 2009). Other structural interpretations, based on finite strain analysis, suggest that the above D_3 to D_4 structures are the product of long-lived Superior-side-up dip–slip (Fueten & Robin 1989), or Superior-side-up transpressional tectonics with a dextral component from *ca.* 1850 to 1750 Ma (Gapais *et al.* 2005, Burnham *et al.* 2009).

THE PIPE II MINE

The Pipe II mine is located approximately 35 km south of Thompson, Manitoba. The mine was operated by Inco Ltd. as an open pit from 1969 to 1984. Clay and silt overburden was removed by dredge prior to mining and exposed extensive outcrops of Ospwagan Group rocks (Bleeker 1990b). Accessible outcrops along the east shoulder of the open pit provide one of the most complete successions of Ospwagan Group rocks in the Thompson Nickel Belt, and make it the type locality of the Pipe Formation (Fig. 2). The ore deposit is situated along the base of a serpentinized ultramafic body emplaced near the base of the Pipe Formation (Bleeker 1990a, 1990b). Intrusion of the ultramafic body occurred at 1880.8 ± 2.5 Ma (Scoates *et al.* 2010); however, little evidence for a contact aureole is present in the Ospwagan Group rocks. Alteration associated with the ultramafic body consists of veins of serpentine, talc, and carbonate that invaded the adjacent country-rocks over the space of a few meters. Simple quartz–feldspar pegmatite dykes up to tens of meters wide and hundreds of meters in length locally intrude both the Archean gneiss and Ospwagan Group stratigraphy. Dykes of granitic pegmatite can be oriented subparallel to the stratigraphy and axial planar to F_2, or oriented axial planar to F_3, and likely represent intrusions of various ages emplaced during metamorphism and deformation.

The rocks at the Pipe II mine are folded into a tight, northeast-trending F_3 synform, plunging steeply toward the east, with a steeply dipping axial plane (Fueten *et al.* 1986, Bleeker 1990a). The stratigraphy of the Ospwagan Group is upward facing, and has been interpreted as the lower upward-facing limb of an F_2 recumbent fold (Bleeker 1990a, Burnham *et al.* 2009). Peak conditions of metamorphism were estimated at 575–625°C, 2.5–5.75 kbar by Fueten *et al.* (1986) on

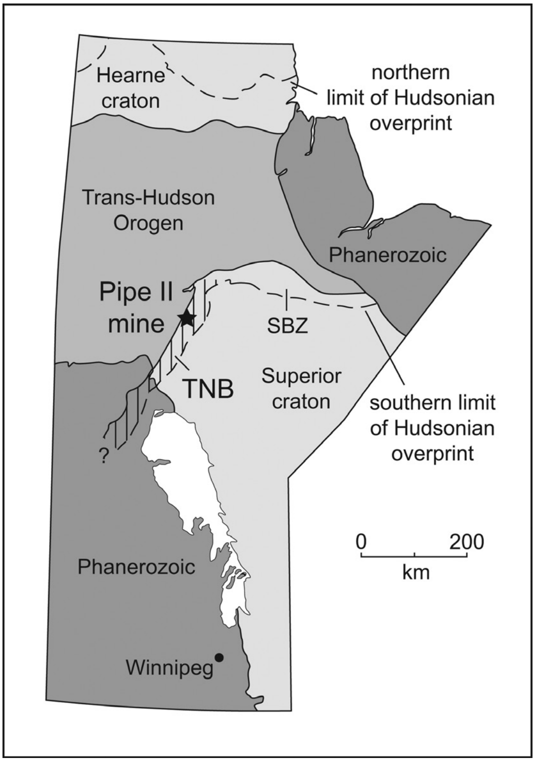

FIG. 1. Simplified tectonic-elements map of Manitoba (adapted from Weber 1990, Burnham *et al.* 2009). The location of the Pipe II mine is indicated with a star. Abbreviations: SBZ: Superior Boundary Zone, TNB: Thompson Nickel Belt.

the basis of metamorphic assemblages and 600–660°C, 5–6 kbar by Bleeker (1990a) using thermobarometric methods. Bleeker (1990a) also recognized the presence of a regional muscovite-out isograd trending through the core area of the synform.

Rocks of the Ospwagan Group are of particular interest because they have only been affected by Hudsonian metamorphism, and because of the presence of metapelitic and metasemipelitic horizons in Manasan, Pipe, and Setting formations, which are ideal for metamorphic investigations. Silicate-facies meta-iron formations from the Pipe Formation were also investigated and have low-variance metamorphic assemblages useful for metamorphic studies.

In order to improve the readability of this text, the "meta" prefix has been dropped from the majority of rock names. However, it should be noted that all rocks investigated in this study have been subjected to amphibolite-facies metamorphic conditions. Mineral assemblages are listed approximately in order of greatest to least abundance.

ANALYTICAL METHODS

The metamorphic grade at the Pipe II mine was established by identifying metamorphic mineral assemblages and using phase-equilibrium modeling. Metamorphic mineral assemblages were identified in outcrop and by detailed petrographic studies (Table 1). Assemblages of interest for further studies were investigated using a JEOL JXA–8200 Superprobe at the University of Calgary Laboratory for Electron Microbeam Analysis (UCLEMA). Carbon-coated thin sections were analyzed using a 20 nA beam at 15 kV and a range of natural and synthetic standards. Amphiboles, feldspars, garnet, orthopyroxene, and staurolite were analyzed by wavelength-dispersive spectroscopy (WDS) with a 5 μm spot-size; biotite and muscovite were analyzed using a 10 μm spot-size. Element-distribution maps of garnet grains were generated using WDS for Mg, Ca, Mn, and Fe to investigate zoning prior to analysis. The garnet grains were then analyzed along automated transects of 10–50 points, perpendicular to the zoning, and passing through the inferred core of the grains. All probe analyses of garnet from iron formations resulted in cation-deficient octahedral sites (*Y* cations) and cation surpluses at the dodecahedral site (*X* cations). This was corrected by calculating a ferric iron (andradite) component using the method of Droop (1987). Representative results of mineral analyses are listed in Tables 2–6.

Samples were sent to Activation Laboratories Ltd. for whole-rock geochemical analysis (Table 7). Concentrations of the major elements were established by lithium metaborite–tetraborate fusion – inductively coupled plasma analysis. Total levels of S and C were established by infrared spectroscopy using an induction furnace for samples suspected of containing significant amounts of sulfide, and to test for the presence of graphite. The proportion of ferrous iron in the iron formations was determined by titration. Phase-equilibrium diagrams were calculated using the THERIAK–DOMINO software package (de Capitani & Brown 1987, de Capitani & Petrakakis 2010), and using the updated ds5.5 thermodynamic dataset of Holland & Powell (1998). Activity models used here are those outlined in Tinkham & Ghent (2005) and Pattison & Tinkham (2009), with the following exceptions: (i) the monoclinic amphibole model is that of Diener *et al.* (2007), (ii) the clinopyroxene model is that of Green *et al.* (2007), (iii) the garnet and biotite models are those of White *et al.* (2007) with the addition of Mn-dominant members that are assumed to mix ideally, (iv) the magnetite–ulvöspinel model is that of White *et al.* (2000), (v) the ilmenite–hematite model is that of White *et al.* (2000), excluding the geikielite component, following Diener *et al.* (2007), and including the pyrophanite component, which is assumed to mix ideally, (vi) the epidote model is that of Holland & Powell (1998), (vii) the liquid model is that of White *et al.* (2007), with the enthalpy of liquids of forsterite and fayalite composition adjusted by –10 kJ/mol and –9 kJ/mol, respectively, following THERMOCALC v.3.31 data files, and (viii) the orthopyroxene model is that of Powell & Holland (1999). Samples were modeled in

TABLE 1. MODAL PERCENTAGE OF ROCK-FORMING MINERALS IN SAMPLES DISCUSSED IN THE TEXT

Area	A	B	B	C	C	D	D	E
Rock	pel	pel	spel	pel	maf	IF sif	IF sif	spel
Sample	PP-08 -08B	PP-06 -27C	PP-08 -13A	PP-06 -28C	PP-06 -26E	PP-06 -29B	PP-06 -24C	PP-07 -01A
And	2.5							
Bt	32.6	34.3	23.0	34.1	18.8	33.9	24.5	27.2
Grt	0.9	2.4		0.8		3.6		
Ilm	1.3	0.8	1.2	tr.	tr.			tr.
Kfs			14.9	11.4		2.0	1.8	4.8
Ms	13.0	13.5	10.1	1.2*				14.0*
Pl	7.6	5.6	16.9	9.8	36.4			8.0
Po	0.9	1.2	tr.	0.4	tr.	2.0	0.3	0.4
Qtz	35.6	25.5	33.9	35.4		22.6	24.7	42.8
Sil	2.4	16.7		6.9				2.8
St	3.2							
Cum/Gru					16.8	19.8	25.9	
Hbl					28.0	0.8	7.7	
Mgt						4.8	0.5	
Opx						10.5	14.6	
Total	100.0	100.0	100.0	100.0	100.0	100.0	100.0	100.0

* Interpreted to be largely a retrograde phase. Symbols: IF sif: silicate facies iron formation, maf: mafic schist, pel: pelite, spel: semipelite, tr.: trace.

FIG. 2. Simplified geological map of the east shoulder of the Pipe II open-pit mine (adapted from Bleeker 1990a). The outlined sample areas, numbered sample locations, and the position of metamorphic isograds are discussed in the text.

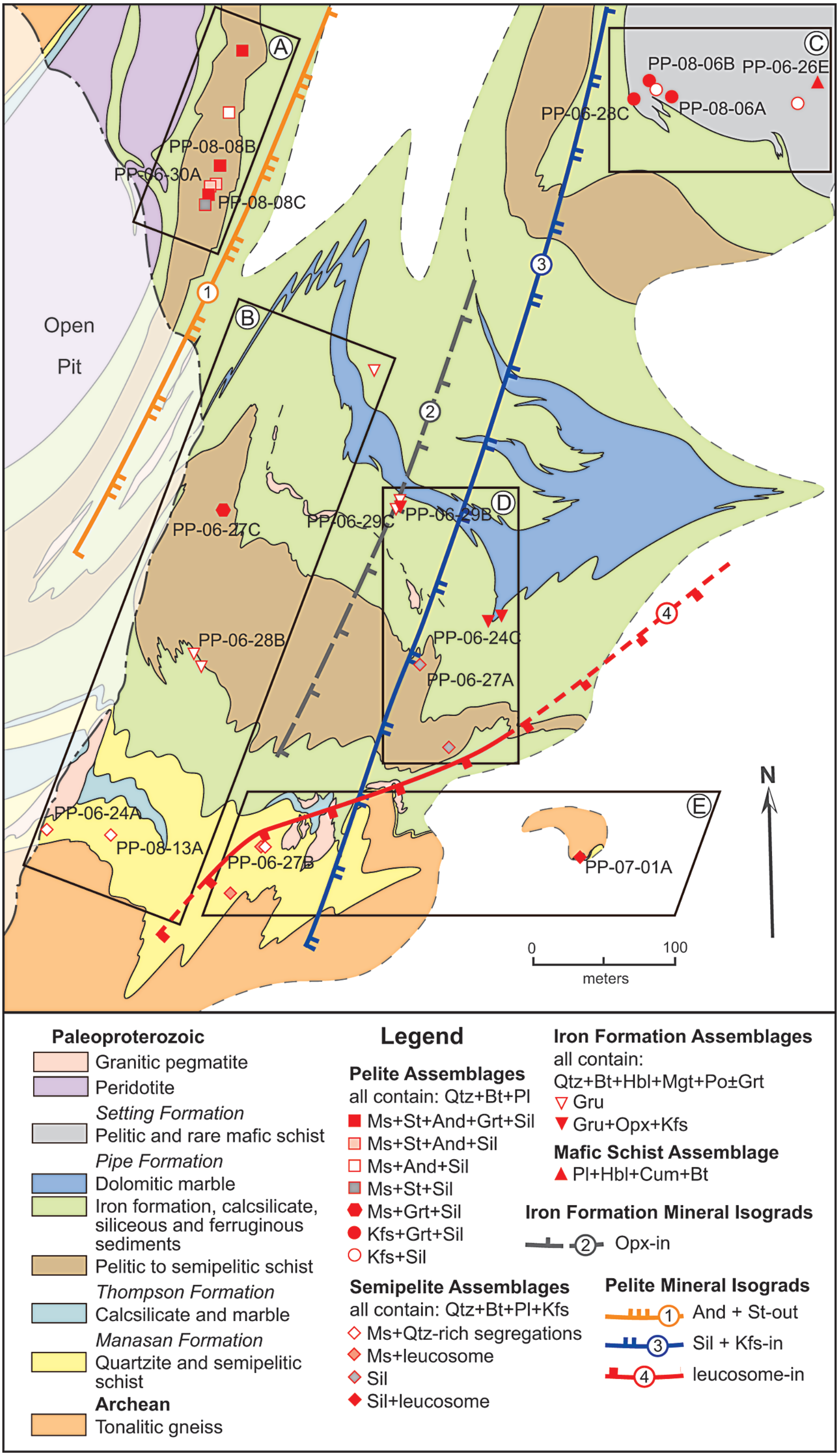
A
B
C
D
E
PP-08-08B
PP-06-30A
PP-08-08C
PP-08-06B
PP-06-26E
PP-08-06A
PP-06-28C
Open
Pit
PP-06-27C
PP-06-29C
PP-06-29B
PP-06-24C
PP-06-27A
PP-06-28B
PP-06-24A
PP-08-13A
PP-06-27B
PP-07-01A
1
2
3
4
N
0
100
meters
Legend
Paleoproterozoic
Granitic pegmatite
Peridotite
Setting Formation
Pelitic and rare mafic schist
Pipe Formation
Dolomitic marble
Iron formation, calcsilicate, siliceous and ferruginous sediments
Pelitic to semipelitic schist
Thompson Formation
Calcsilicate and marble
Manasan Formation
Quartzite and semipelitic schist
Archean
Tonalitic gneiss
Pelite Assemblages
all contain: Qtz+Bt+Pl
Ms+St+And+Grt+Sil
Ms+St+And+Sil
Ms+And+Sil
Ms+St+Sil
Ms+Grt+Sil
Kfs+Grt+Sil
Kfs+Sil
Semipelite Assemblages
all contain: Qtz+Bt+Pl+Kfs
Ms+Qtz-rich segregations
Ms+leucosome
Sil
Sil+leucosome
Iron Formation Assemblages
all contain:
Qtz+Bt+Hbl+Mgt+Po±Grt
Gru
Gru+Opx+Kfs
Mafic Schist Assemblage
Pl+Hbl+Cum+Bt
Iron Formation Mineral Isograds
2 Opx-in
Pelite Mineral Isograds
1 And + St-out
3 Sil + Kfs-in
4 leucosome-in

the chemical system MnNCKFMASHT ($MnO–Na_2O–CaO–K_2O–FeO–MgO–Al_2O_3–SiO_2–H_2O–TiO_2$, with C and P_2O_5 omitted from the whole-rock analysis, and projected from pyrrhotite). The chemical system was oversaturated with a pure H_2O fluid phase below the solidus. Above the solidus, the H_2O content of each model is restricted to the amount of H_2O contained in the solid phases at 7 kbar and <0.5°C below the solidus. The H_2O content in the system at the temperature of melting is therefore at the point of saturation (White *et al.* 2001).

Migmatitic rocks are by their nature compositionally heterogeneous. Heterogeneity arises when partial melts begin to pool and migrate through the rock. To obtain a meaningful bulk composition for the migmatitic semipelite, a sample was chosen where the rock featured relatively small pools of leucosome, and an absence of injected veins. Bulk-rock geochemical analyses of the non-migmatitic Manasan Formation semipelite (PP–08–13A) and the migmatitic Manasan formation (PP–07–01A) indicate very similar compositions (Table 7), and the calculated equilibrium-assemblage diagrams are nearly identical. The results suggest that the bulk-rock composition of the migmatitic semipelite is representative of the rock prior to partial melting.

Samples of iron formation were modeled with ferric iron as an additional component. Orthopyroxene and grunerite from iron formations are typically Mn-bearing (*cf.* Immega & Klein 1976, Bohlen *et al.* 1980) and, in extreme cases, may contain up to 17 and 15 wt% MnO, respectively (Klein 1966, Krogh 1977). Bohlen *et al.* (1980) demonstrated that Mn increases the stability field of Fe-rich orthopyroxene. Therefore, to provide a comparative assessment of these effects, the iron formation and mafic schist were modeled in the following systems: (1) the Mn-free system NCKFMASHT(O), (2) MnNCKFMASHT(O), utilizing Mn-bearing solid solutions for the phases garnet, biotite, ilmenite, chlorite, cordierite, and staurolite, and (3) MnNCKFMASHT(O), the same as (2), but with the phase component rhodonite added to the orthopyroxene solution-model. Although rhodonite is not a pyroxene-group mineral, as a pyroxenoid it is one of the closest analogues to a Mn pyroxene available in the thermodynamic dataset of Holland & Powell (1998). Ideally, the Mn-dominant orthopyroxene donpeacorite would be used (Petersen *et al.* 1984, Morimoto 1989); however, limited thermodynamic data are currently available for this phase (Graphchikov 1992, Stimpfl 2005). For simplicity, the rhodonite component is assumed to form an ideal solution with equipartitioning of Mn into both octahedral sites (*cf.* Bohlen *et al.* 1980).

The compositions of the samples of iron formation studied here have high Fe/(Fe + Mg) values, whereas

TABLE 2. REPRESENTATIVE COMPOSITIONS OF BIOTITE IN SAMPLES DISCUSSED IN THE TEXT

Area	A	B	B	C	C	D	D
Rock type	pel	pel	IF sif	pel	maf	IF sif	IF sif
Sample	PP-08-08B	PP-06-27C	PP-06-28A	PP-06-28C	PP-06-26E	PP-06-24C	PP-06-29B
SiO_2 wt%	34.05	34.82	33.30	34.44	37.77	33.34	33.53
TiO_2	1.60	1.92	2.17	2.53	2.60	0.81	0.77
Al_2O_3	19.58	19.46	14.99	19.24	15.12	15.80	14.43
FeO	21.81	21.82	32.69	21.79	17.15	32.27	32.80
MnO	0.05	0.06	0.01	0.19	0.05	0.23	0.15
MgO	7.99	7.23	4.04	7.81	14.91	3.58	5.59
CaO	0.01	0.01	0.03	b.d.l.	0.03	0.07	0.07
Na_2O	0.24	0.20	0.11	0.07	0.32	0.02	0.19
K_2O	8.81	9.39	8.24	9.37	8.32	9.00	7.97
Total	94.14	94.91	95.73[a]	95.44	96.44[b]	95.12	95.54[c]
Si *apfu*	5.306	5.387	5.420	5.307	5.594	5.466	5.459
^{IV}Al	2.694	2.613	2.580	2.693	2.406	2.534	2.541
^{VI}Al	0.902	0.936	0.294	0.801	0.234	0.519	0.229
Ti	0.188	0.223	0.266	0.293	0.290	0.100	0.094
Fe^{2+}	2.842	2.823	4.450	2.808	2.125	4.424	4.466
Mn	0.007	0.008	0.002	0.025	0.006	0.032	0.021
Mg	1.857	1.668	0.979	1.795	3.293	0.876	1.357
Ca	0.002	0.001	0.004	0.000	0.005	0.012	0.012
Na	0.071	0.060	0.036	0.022	0.092	0.005	0.059
K	1.752	1.852	1.711	1.842	1.571	1.883	1.656
Total	15.621	15.571	15.742	15.586	15.616	15.851	15.894
Mg#	0.40	0.37	0.18	0.39	0.61	0.17	0.23

Cation proportions, in atoms per formula unit (*apfu*), are calculated on the basis of 22 atoms of oxygen. Mg#: Mg/(Mg + Fe); b.d.l.: below detection limit. [a] includes 0.15 wt% BaO, [b] includes 0.17 wt% BaO, [c] includes 0.04 wt% BaO.

TABLE 3. REPRESENTATIVE COMPOSITIONS OF FELDSPAR IN SAMPLES DISCUSSED IN THE TEXT

Area	A	B	C	C	C	D	D
Rock type	pel	pel	pel	pel	maf	IF sif	IF sif
Sample	PP-08-08B	PP-06-27C	PP-06-28C	PP-06-28C	PP-06-26E	PP-06-24C	PP-06-29B
	Pl	Pl	Pl	Kfs	Pl	Kfs	Kfs
SiO_2 wt%	60.59	61.22	61.85	63.96	61.59	63.75	64.69
Al_2O_3	24.46	24.09	24.44	19.21	25.06	18.70	18.89
FeO	0.13	0.02	0.03	0.01	0.08	0.05	0.20
CaO	4.32	4.54	5.35	0.02	5.62	0.01	b.d.l.
Na_2O	8.89	8.71	7.61	1.07	8.35	0.69	0.71
K_2O	0.04	0.10	0.21	14.99	0.07	15.77	16.06
Total	98.43	98.68	99.49	99.26	100.79[a]	98.97	100.91[b]
Si *apfu*	2.726	2.745	2.746	2.966	2.711	2.976	2.974
^{IV}Al	1.297	1.273	1.279	1.050	1.300	1.029	1.024
Fe^{2+}	0.005	0.001	0.001	0.000	0.003	0.002	0.007
Ca	0.208	0.218	0.255	0.001	0.265	0.001	0.000
Na	0.775	0.757	0.655	0.096	0.712	0.062	0.063
K	0.003	0.006	0.012	0.887	0.004	0.939	0.942
Total	5.014	5.000	4.948	5.000	4.995	5.009	5.010
*X*An mol.%	0.21	0.22	0.28	0.00	0.27	0.00	0.00
*X*Ab	0.79	0.77	0.71	0.10	0.73	0.06	0.06
*X*Or	0.00	0.01	0.01	0.90	0.00	0.94	0.94

Cation proportions, in atoms per formula unit (*apfu*), are calculated on the basis of eight atoms of oxygen. b.d.l.: below detection limit. [a] includes 0.02 wt% BaO, [b] includes 0.36 wt% BaO.

TABLE 4. REPRESENTATIVE COMPOSITIONS OF GARNET IN SAMPLES DISCUSSED IN THE TEXT

Area	A	A	B	B	B	B	C	C	D	D
Rock type	pel	pel	pel	pel	IF sif	IF sif	pel	pel	IF sif	IF sif
Sample	PP-08 -08B Grt c	PP-08 -08B Grt r	PP-06 -27C Grt c	PP-06 -27C Grt r	PP-06 -28A Grt c	PP-06 -28A Grt r	PP-06 -28C Grt c	PP-06 -28C Grt r	PP-06 -29B Grt c	PP-06 -29B Grt r
SiO_2 wt%	37.10	36.96	37.58	37.50	36.01	36.97	36.82	36.62	36.38	36.00
TiO_2	0.02	0.03	b.d.l.	0.03	b.d.l.	b.d.l.	0.01	0.02	0.04	b.d.l.
Al_2O_3	20.67	20.50	21.01	21.19	20.00	20.04	20.25	20.15	19.72	20.31
Fe_2O_3	--	--	--	--	2.77	1.57	--	--	2.69	3.06
FeO	35.77	37.29	33.95	36.21	34.24	33.93	32.12	33.23	33.61	29.91
MnO	3.78	3.01	5.71	3.75	1.28	0.83	6.79	6.55	4.50	4.33
MgO	2.19	2.22	2.30	2.13	0.61	0.46	2.60	2.01	0.95	0.63
CaO	1.46	1.27	1.13	1.23	5.02	6.72	1.16	0.96	2.87	5.96
Total	101.01[a]	101.28	101.72[b]	102.06[c]	99.93	100.52	99.76[d]	99.56[e]	100.76	100.20
Si *apfu*	2.993	2.984	3.002	2.991	2.949	2.995	3.001	3.005	2.967	2.932
^{IV}Al	0.007	0.016	0.000	0.009	0.051	0.005	0.000	0.000	0.033	0.068
^{VI}Al	1.959	1.935	1.978	1.982	1.880	1.909	1.946	1.948	1.863	1.881
Fe^{3+}	--	--	--	--	0.171	0.096	--	--	0.165	0.187
Ti	0.001	0.002	0.000	0.001	0.000	0.000	0.000	0.001	0.002	0.000
Fe^{2+}	2.413	2.518	2.268	2.415	2.346	2.299	2.190	2.280	2.292	2.037
Mn	0.258	0.206	0.386	0.253	0.089	0.057	0.469	0.455	0.311	0.299
Mg	0.264	0.268	0.274	0.253	0.074	0.056	0.316	0.246	0.116	0.076
Ca	0.126	0.110	0.097	0.105	0.441	0.584	0.101	0.084	0.251	0.520
Total	8.021	8.039	8.005	8.009	8.001	8.001	8.023	8.019	8.000	8.000
Mg#	0.10	0.10	0.11	0.09	0.03	0.02	0.13	0.10	0.05	0.03
*X*Grs	0.04	0.04	0.03	0.03	0.07	0.15	0.03	0.03	0.00	0.09
*X*Sps	0.08	0.07	0.13	0.08	0.03	0.02	0.15	0.15	0.10	0.10
*X*Alm	0.79	0.81	0.75	0.80	0.80	0.77	0.71	0.74	0.77	0.69
*X*Prp	0.09	0.09	0.09	0.08	0.03	0.02	0.10	0.08	0.04	0.03
*X*Adr					0.08	0.05			0.08	0.09

Cation proportions, in atoms per formula unit (*apfu*), are calculated on the basis of 12 atoms of oxygen. The proportion of Fe_2O_3 calculated using the method of Droop (1987). Mg#: Mg/(Mg + Fe); b.d.l.: below detection limit; c: core, r: rim, –: not calculated. [a] includes 0.02 wt% Cr_2O_3, [b] includes 0.04 wt% Cr_2O_3, [c] includes 0.02 wt% Cr_2O_3, [d] includes 0.01 wt% Cr_2O_3, and [e] includes 0.02 wt% Cr_2O_3.

the amphibole model of Diener *et al.* (2007) is defined dominantly in terms of Mg-dominant members and only one ferrous iron member. This combination caused algorithmic convergence problems during Gibbs minimization, and the amphibole model was therefore transformed to a different set of independent components, containing additional ferrous iron members, using the model outlined in Powell & Holland (1999). No end-member data were available for Mn-bearing minerals of the amphibole, epidote, or magnetite groups.

MINERAL ASSEMBLAGES

Key mineral assemblages in pelites, semipelites, and iron formations were identified in several areas (labeled A–E in Fig. 2). A variety of iron formations are present including carbonate-, silicate-, sulfide-, and rare oxide-facies iron formations. Individual layers of iron formation are typically intermediate between these end-members. Iron formations with carbonate were not included in the study in an attempt to minimize the effects of varying compositions of metamorphic fluid. Variable amounts of biotite, garnet, and locally feldspar suggest there is a clastic component to the iron formations (Klein 2005, Zwanzig *et al.* 2007). The iron formations are generally mesobanded (banding 1.7–24.5 mm thick, Klein 2005), and quartz-rich (metachert) layers are common. A horizon of mafic schist, containing coexisting Mg–Fe and Ca clinoamphiboles from within the Setting Formation was also sampled. Foliation S_2 is the dominant one in all samples, and it is parallel to the stratigraphic layering (S_0).

Area A

The Pipe Formation pelite in area A consists of a fine-grained schist that is locally protomylonitic. The schist is characterized by the assemblage Qtz + Ms + Bt + Pl + Sil with or without St, Grt, and And. Accessory graphite and pyrrhotite are common. The

TABLE 5. REPRESENTATIVE COMPOSITIONS OF AMPHIBOLE IN SAMPLES DISCUSSED IN THE TEXT

Area	B	B	C	C	D	D	D	D	D
Rock type	IF sif	IF sif	maf	maf	IF sif	IF sif	IF sif	IF sif	IF sif
Sample	PP-06-28A	PP-06-28A	PP-06-26E	PP-06-26E	PP-06-24C	PP-06-24C	PP-06-24C	PP-06-29B	PP-06-29B
	Gru	Hbl	Cum	Hbl	Gru p	Gru r	Hbl	Gru	Hbl
SiO_2 wt%	49.34	38.72	54.16	49.55	49.52	48.54	40.39	50.46	41.18
TiO_2	0.02	0.43	0.04	0.61	0.03	0.03	0.17	b.d.l.	0.12
Al_2O_3	0.74	13.12	0.61	7.05	0.43	0.32	11.54	0.50	10.70
FeO	43.18	29.99	24.27	13.78	40.68	44.01	30.03	39.70	29.51
MnO	0.18	0.02	0.60	0.21	2.01	1.56	0.64	1.13	0.26
MgO	4.42	1.90	18.45	14.63	5.14	2.68	2.91	6.82	3.65
CaO	0.56	10.99	1.01	11.33	0.51	0.43	10.31	0.40	10.62
Na_2O	0.12	1.65	0.06	0.87	0.10	0.04	1.59	0.12	1.57
K_2O	0.02	0.93	0.02	0.15	0.01	b.d.l.	1.26	0.03	1.33
Total	98.58	97.75	99.22	98.18	98.43	97.61	98.84	99.16	98.94
Si *apfu*	7.903	6.220	7.839	7.163	7.917	7.956	6.415	7.911	6.507
^{IV}Al	0.097	1.780	0.104	0.837	0.081	0.044	1.585	0.089	1.493
^{VI}Al	0.043	0.703	0.000	0.365	0.000	0.018	0.575	0.004	0.500
Ti	0.003	0.052	0.004	0.067	0.004	0.004	0.020	0.000	0.014
Mg	1.055	0.456	3.981	3.154	1.224	0.655	0.690	1.595	0.860
Fe^{2+}	5.784	4.029	2.938	1.666	5.439	6.033	3.989	5.205	3.901
Mn	0.024	0.002	0.074	0.026	0.272	0.216	0.086	0.150	0.034
Ca	0.096	1.892	0.157	1.755	0.087	0.076	1.754	0.067	1.798
Na	0.036	0.512	0.016	0.245	0.015	0.006	0.488	0.035	0.481
K	0.003	0.190	0.003	0.029	0.001	0.000	0.255	0.006	0.268
Total	15.044	15.836	15.116	15.307	15.040	15.008	15.857	15.062	15.856
Mg#	0.15	0.10	0.58	0.65	0.18	0.10	0.15	0.23	0.18

Cation proportions, in atoms per formula unit (*apfu*), are calculated on the basis of 23 atoms of oxygen. Mg#: Mg/(Mg + Fe), b.d.l.: below detection limit. p: prograde, r: retrograde.

S_2 wraps around porphyroblasts of both andalusite and staurolite. Grains of garnet are idioblastic with few inclusions. Although there is a weak sense of S_2 wrapping garnet porphyroblasts, small grains of garnet locally overgrow the S_2 foliation (Fig. 3a). The garnet is characterized by rather simple chemical zoning profiles of Ca, Mn, and Mg/(Fe + Mg) (Mg#, Fig. 4). Staurolite partially replaced by andalusite, sillimanite, or biotite is common, suggesting the reaction:

$$\mathrm{Ms + St + Qtz = Bt + Al_2SiO_5 + H_2O}. \qquad (1)$$

Patchy intergrowths of biotite and fibrous sillimanite wrapped by S_2 are not uncommon and may represent pseudomorphs of staurolite (Fig. 3b). Fibrous sillimanite and, rarely, fine prismatic sillimanite, have locally replaced andalusite porphyroblasts in pressure shadows (Fig. 3c), indicating passage from the andalusite to sillimanite field of stability.

A later S_3 foliation cuts across the S_2 foliation. It is composed of fine- to very fine-grained biotite, sillimanite, muscovite, and quartz (Fig. 3d). The S_3 foliation wraps all the previously mentioned porphyroblasts and locally cuts across staurolite grains. Randomly oriented coarse- to very coarse-grained muscovite locally rims both staurolite and andalusite porphyroblasts. Evidence for retrograde metamorphism is present as partial replacement of staurolite by chlorite along grain boundaries and fractures, and partially chloritized biotite grains.

Area B

The Pipe Formation pelite in area B contains the assemblage Qtz + Bt + Ms + Pl + Sil with or without Grt. Where present, garnet forms hypidiomorphic porphyroblasts wrapped by S_2. Rarely, idioblastic faces on garnet grains appear to overgrow the S_2 foliation. The chemical zoning profiles of the garnet are relatively simple (Fig. 5). Masses of fibrous sillimanite intergrown with biotite, similar to those in pelites from area A, may represent pseudomorphs of staurolite.

The Manasan Formation semipelite from area B contain the assemblage Qtz + Ms + Pl + Bt + Kfs. Outcrops consist of intensely folded schist with preserved sedimentary layering (Fig. 3e). The groundmass of the schist consists of fine-grained quartz, plagioclase, and microcline. Millimeter- to cm-thick leucocratic segregations are abundant in this unit (Figs. 3e, f). They are oriented parallel to the compositional layering and are characterized by sharp boundaries with melanocratic selvedges. The segregations consist dominantly of coarse-grained quartz with minor microcline and are intensely boudinaged and folded. The quartz in the segregations has sutured grain-boundaries, and the microcline occurs as discrete grains distributed along the margin of the segregations (Fig. 3h). Boudinaged segments are wrapped by S$_2$, whereas the fold axes are parallel to an S$_3$ crenulation in the rock. Local S$_3$ shear bands of mylonitic biotite, muscovite, and quartz are planar to the crenulations and transect the segregations. The absence of sillimanite and the presence of groundmass microcline along with abundant prograde muscovite suggest that microcline was an original detrital component of the sediment. The following characteristics of the quartz-rich segregations suggest that they formed under subsolidus conditions (Sawyer & Robin 1986, Sawyer 2008): (i) the segregations occur parallel to the compositional layering of the semipelite, and are most commonly present at the interface between layers of differing composition and potentially differing rheology, (ii) the segregations have sharp contacts with the host semipelite mantled by melanocratic selvedges, (iii) the segregations are composed of dominantly quartz with minor K-feldspar, far from a cotectic melt composition, (iv) microcline is typically present along the margins of the segregations and not randomly distributed throughout, (v) the quartz-dominated segregations behaved competently prior to being folded plastically, suggesting that at least some of the segregations existed while temperatures were less than *ca.* 310°C during the prograde evolution of the rock (Stöckhert *et al.* 1999).

TABLE 6. REPRESENTATIVE COMPOSITIONS OF MINERALS IN SAMPLES DISCUSSED IN THE TEXT

Area	A	A	B	C	D	D
Rock type	pel	pel	pel	pel	IF sif	IF sif
Sample	PP-08 -08B	PP-08 -08B	PP-06 -27C	PP-06 -28C	PP-06 -24C	PP-06 -29B
	St	Ms	Ms	Ms	Opx	Opx
SiO$_2$ wt%	26.03	46.04	47.00	45.32	47.54	47.42
TiO$_2$	0.38	0.31	0.36	0.55	b.d.l.	0.01
Al$_2$O$_3$	56.45	37.19	36.25	35.85	0.18	0.15
FeO	14.31	1.07	1.10	1.28	45.95	44.78
MnO	0.17	--	--	b.d.l.	2.70	1.73
MgO	1.10	0.37	0.46	0.51	4.31	6.03
CaO	b.d.l.	0.01	b.d.l.	0.01	0.71	0.62
Na$_2$O	--	1.28	0.55	0.39	b.d.l.	b.d.l.
K$_2$O	--	9.33	10.28	10.46	--	0.02
Total	98.74^{a}	95.60	96.00	94.37	101.39	100.76
Si *apfu*	7.195	6.067	6.180	6.097	1.990	1.980
^{IV}Al	0.805	1.933	1.820	1.903	0.009	0.008
^{VI}Al	17.588	3.843	3.797	3.758	0.000	0.000
Ti	0.080	0.031	0.035	0.051	0.000	0.000
Fe^{2+}	3.308	0.118	0.121	0.147	1.609	1.564
Mn	0.025	--	--	0.000	0.096	0.061
Mg	0.452	0.072	0.090	0.111	0.269	0.375
Ca	0.000	0.002	0.000	0.000	0.032	0.028
Na	--	0.327	0.139	0.116	0.000	0.000
K	--	1.568	1.725	1.792	--	0.001
Total	29.453	13.961	13.907	13.975	4.005	4.017
Mg#	0.12				0.14	0.19

Cation proportions, in atoms per formula unit (*apfu*), are calculated on the basis of 46 atoms of oxygen for staurolite, 22 atoms of oxygen for muscovite, and six atoms of oxygen for orthopyroxene. Mg#: Mg/(Mg + Fe); b.d.l.: below detection limit, –: not analyzed. ^{a} includes 0.30 wt% ZnO.

The silicate-facies iron formations of the Pipe Formation from area B typically contain the mineral assemblage Qtz + Grt + Gru + Bt + Hbl + Po + Mgt. Rock textures are variable and range from granoblastic in relatively biotite-poor rocks to foliated in biotite-rich rocks. Grunerite is generally granoblastic; however, local elongate grains are oriented parallel to S$_2$. Exsolution lamellae of hornblende within grunerite, and of grunerite within hornblende, are common. Garnet is generally idioblastic to hypidioblastic and wrapped by the S$_2$ foliation. Garnet grains can be fractured parallel to S$_2$ and infilled by quartz. Garnet growth appears to have occurred at various times depending on the compositional band. Dark green hornblende defines a strong L$_2$ lineation within the S$_2$ foliation. A local, weak S$_3$ foliation consists of reoriented grains of biotite and grunerite.

Area C

The pelitic assemblages of the Setting Formation in area C contain Qtz + Bt + Sil + Kfs + Pl + Ms with or without Grt. Outcrops are speckled by ubiquitous knots of sillimanite and can be banded owing

TABLE 7. WHOLE-ROCK COMPOSITIONS OF SAMPLES DISCUSSED IN THE TEXT

Area	A	B	B	C	C	D	E
Rock	pel	pel	spel	pel	maf	IF sif	spel
Sample	PP-08 -08B	PP-06 -27C	PP-08 -13A	PP-06 -28C	PP-06 -26E	PP-06 -29B	PP-07 -01A
SiO$_2$ wt%	65.11	62.87	67.82	67.56	52.87	53.60	71.44
Al$_2$O$_3$	16.93	18.40	14.93	16.39	12.66	6.37	13.85
Fe$_2$O$_3$T	6.49	8.02	5.42	6.42	11.37	--	4.98
Fe$_2$O$_3$	--	--	--	--	--	5.39	--
FeO	--	--	--	--	--	22.40	--
MnO	0.042	0.075	0.038	0.078	0.178	0.702	0.032
MgO	1.91	2.21	1.49	1.85	9.58	3.57	1.26
CaO	0.97	0.56	0.53	0.78	5.19	0.95	0.34
Na$_2$O	1.88	1.21	0.64	1.60	3.34	0.14	0.57
K$_2$O	3.63	4.18	6.35	4.47	1.41	3.14	4.78
TiO$_2$	0.482	0.579	0.739	0.752	0.923	0.214	0.719
P$_2$O$_5$	0.08	0.04	0.07	0.05	0.07	0.25	0.06
LOI	3.06	2.21	1.78	0.89	0.83	2.04	1.58
Total	100.58	100.35	99.81	100.84	98.42	98.77	99.61
S	0.215	0.347	0.010	0.055	0.013	0.440	0.122
C	0.27	0.30	0.05	0.03	0.01	0.13	0.02
Mg#	0.37	0.35	0.35	0.36	0.63	0.19	0.33
Mn#	0.005	0.007	0.005	0.009	0.007	0.021	0.005

All consituents are reported in wt%. Total Fe is reported as Fe$_2$O$_3$T. Mg#: Mg/(Mg + Fe), Mn#: Mn/(Mn + Mg + Fe). Symbols: IF sif: silicate facies iron formation, maf: mafic schist, pel: pelite, spel: semipelite, –: not reported.

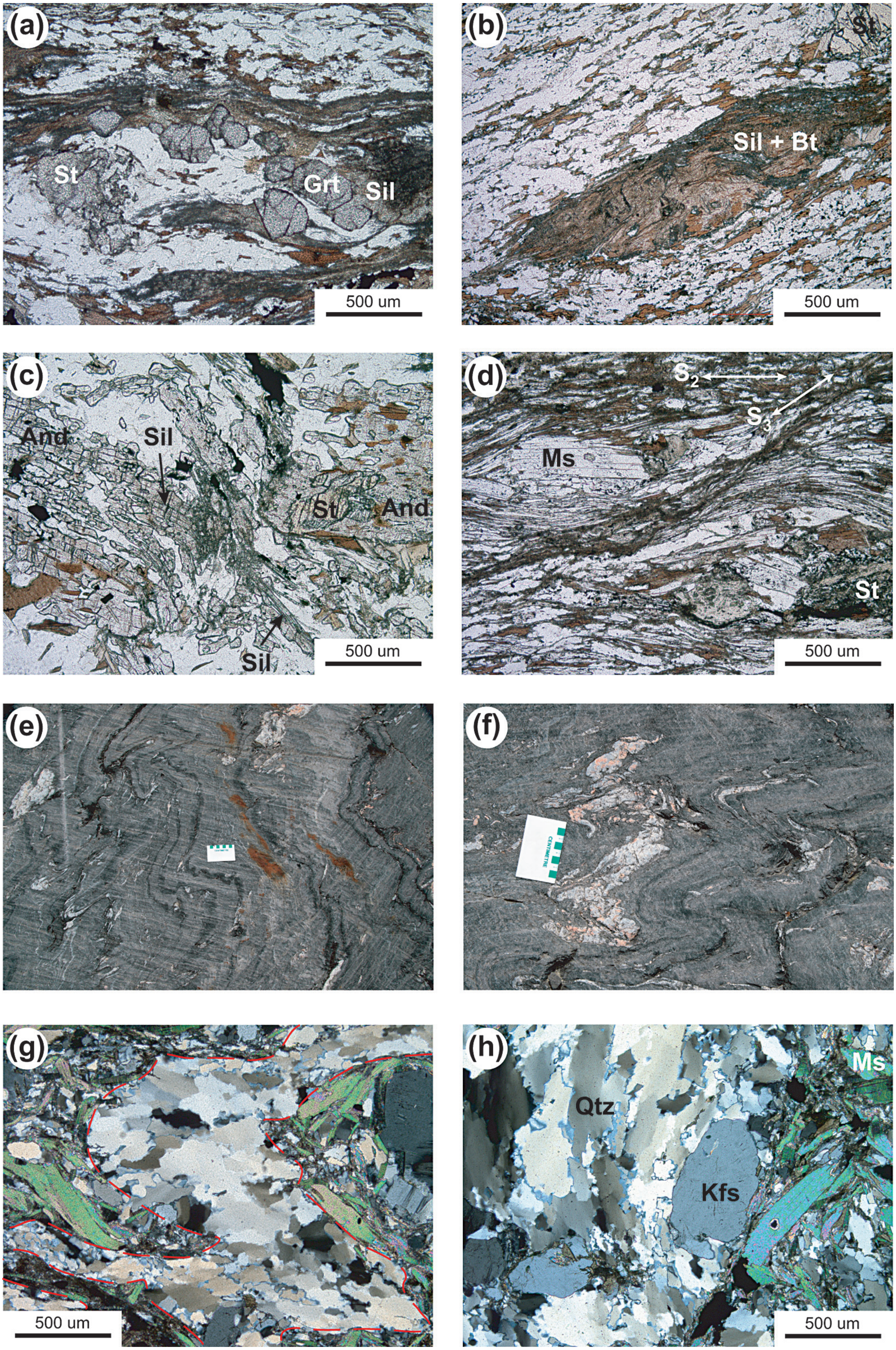
(a)
St
Grt
Sil
500 um
(b)
St
Sil + Bt
500 um
(c)
And
Sil
St
And
Sil
500 um
(d)
S_2
S_3
Ms
St
500 um
(e)
(f)
CENTIMETRE
(g)
500 um
(h)
Qtz
Kfs
Ms
500 um

to preserved sedimentary bedding (S_0) (Figs. 6a, b). Medium-grained biotite, along with rare muscovite, define the S_2 foliation. The knots of fibrous sillimanite are generally flattened parallel to S_2. Where present, garnet forms xenomorphic to hypidiomorphic porphyroblasts elongate parallel to, and wrapped by, the S_2 foliation. Potassium feldspar forms equant, xenomorphic porphyroblasts with inclusions of biotite, quartz, and rare muscovite (Fig. 6c). Inclusions of biotite and muscovite are commonly oriented, suggesting that the microcline overgrew the S_2 foliation. The general lack of prograde muscovite and an abundance of sillimanite and K-feldspar suggest the reaction:

$$\text{Ms} + \text{Qtz} = \text{Sil} + \text{Kfs} + \text{H}_2\text{O or melt}. \quad (2)$$

There is a distinct lack of leucosome development. The equant nature of the K-feldspar and its random distribution within the matrix of the rock suggest that melt was not generated by reaction (2), and that the K-feldspar formed through solid-state reactions.

An S_3 foliation is locally defined by the reorientation of sillimanite fibers within S_2-flattened sillimanite knots (Fig. 6d) and by the reorientation of micas. Late, coarse-grained muscovite can also replace sillimanite knots and K-feldspar (Fig. 6c). Discrete zones of retrograde metamorphism, up to several centimeters thick, occur along fractures that cut across the outcrops in area C. Sillimanite knots within the zones are replaced by very fine-grained white mica, biotite is replaced by chlorite, and coarse-grained muscovite becomes more common. Garnet is largely replaced by chlorite along fractures and grain boundaries, and plagioclase is moderately converted to a white mica. In contrast, the K-feldspar is unaltered and can contain inclusions of unaltered biotite.

A horizon of mafic schist, tentatively interpreted as reworked volcanic deposits, occurs within Setting Formation rocks in Area C. It contains the assemblage Pl + Hbl + Cum + Bt. The rock is laminated to layered and moderately foliated. Plagioclase is granoblastic and commonly untwinned. Biotite is locally reoriented into a later S_3 foliation, which cross-cuts S_2. Hornblende and cummingtonite commonly occur as single-grain intergrowths observed by petrographic microscope (Fig. 6e), and as cryptic exsolution-induced lamellae within each other detected in back-scattered electron images. Both amphiboles are generally granoblastic, but can be elongate parallel to S_2, and both amphiboles are locally cut by S_3 and reoriented parallel to it.

FIG. 3. Photomicrographs of pelite from the Pipe Formation in area A showing: (a) small garnet porphyroblasts overgrowing S_2 sillimanite and micas (sample PP–08–08B); (b) mass of very fine-grained biotite and fibrous sillimanite, possibly a pseudomorph of staurolite (sample PP–06–30A); (c) staurolite overgrown by andalusite, and andalusite overgrown by fine prismatic sillimanite (sample PP–08–08B), and (d) S_3 foliation comprised of very fine-grained muscovite, biotite, and sillimanite cutting across the dominant S_2 foliation (sample PP–08–08C). Outcrop photographs of semipelite from the Manasan Formation showing: (e) folded primary bedding and (f) bedding-parallel quartz-rich segregations. Scale card is in centimeters. Photomicrographs from the above semipelite showing: (g) a folded quartz-rich segregation, and (h) coarse-grained microcline in a quartz-rich segregation (sample PP–06–24A).

Area D

The semipelite rocks of the Pipe Formation from area D contain the prograde assemblage Qtz + Bt + Pl + Sil + Kfs. They are similar to the pelitic rocks of the Setting Formation documented from area C, with ubiquitous knots of sillimanite, porphyroblasts of K-feldspar, and muscovite that is interpreted as a retrograde mineral.

The silicate-facies iron formation of the Pipe Formation from area D is locally orthopyroxene-bearing and contains the assemblage Qtz + Bt + Gru + Opx + Hbl + Mgt +Kfs + Po ± Grt. Orthopyroxene can occur as the product of grunerite dehydration:

$$\text{Gru} = \text{Opx} + \text{Qtz} + \text{H}_2\text{O} \quad (3)$$

or through decarbonation of siderite (Klein 2005):

$$\text{Sd} + \text{Qtz} = \text{Opx} + \text{CO}_2 \quad (4)$$

Reaction (3) is the favored origin for the orthopyroxene, as grunerite-bearing and orthopyroxene-free iron formations are common in area B, and carbonate-free iron formations were selected specifically for this study; however, several horizons of Fe-carbonate-bearing iron formations are present farther up-section, so reaction (4) cannot be discounted.

Orthopyroxene locally appears to have overgrown the S_2 fabric. Optically continuous overgrowths of grunerite on hornblende are common, as are exsolution lamellae of grunerite in hornblende and lamellae of hornblende in grunerite (Fig. 6f). Exsolution lamellae of hornblende in grunerite suggest that the grunerite is a part of the prograde assemblage and not retrograde after orthopyroxene (Kahl & Schumacher 2000). Fine-grained, rounded K-feldspar occurs in the typically quartz-rich groundmass, which is wrapped by S_2. Garnet is characterized by rather simple chemical zoning, and as expected, is Fe-rich (Fig. 7). Very fine-grained biotite, grunerite, and quartz define S_3 shear bands that transect S_2. Orthopyroxene, hornblende, and garnet are wrapped by S_3. Very fine-grained grunerite also locally replaces orthopyroxene along grain boundaries (Fig. 6g). This fine-grained grunerite is interpreted as retrograde through the back-reaction of reaction (3). The Mg# of prograde grunerite (0.18) in sample

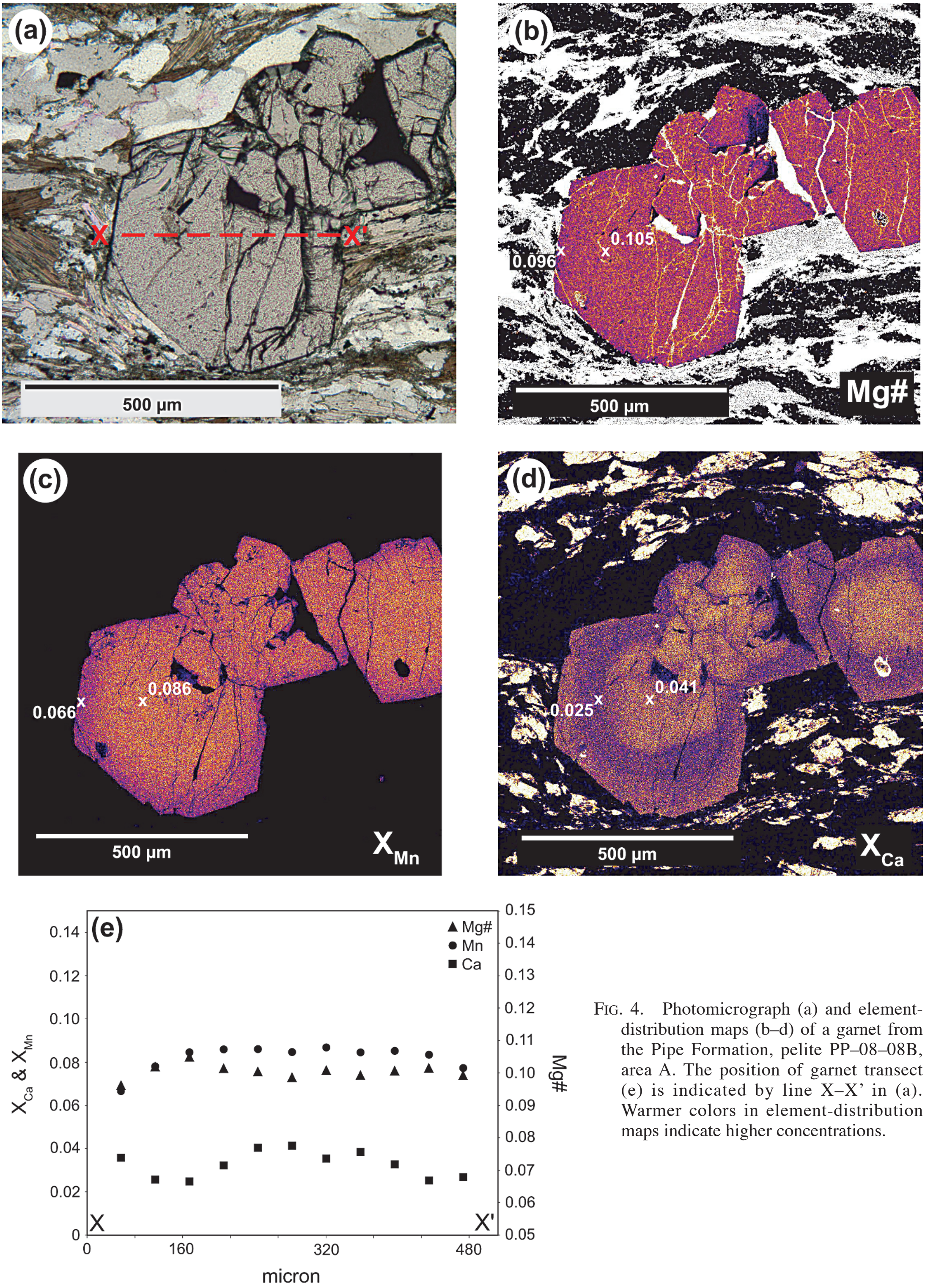

FIG. 4. Photomicrograph (a) and element-distribution maps (b–d) of a garnet from the Pipe Formation, pelite PP–08–08B, area A. The position of garnet transect (e) is indicated by line X–X' in (a). Warmer colors in element-distribution maps indicate higher concentrations.

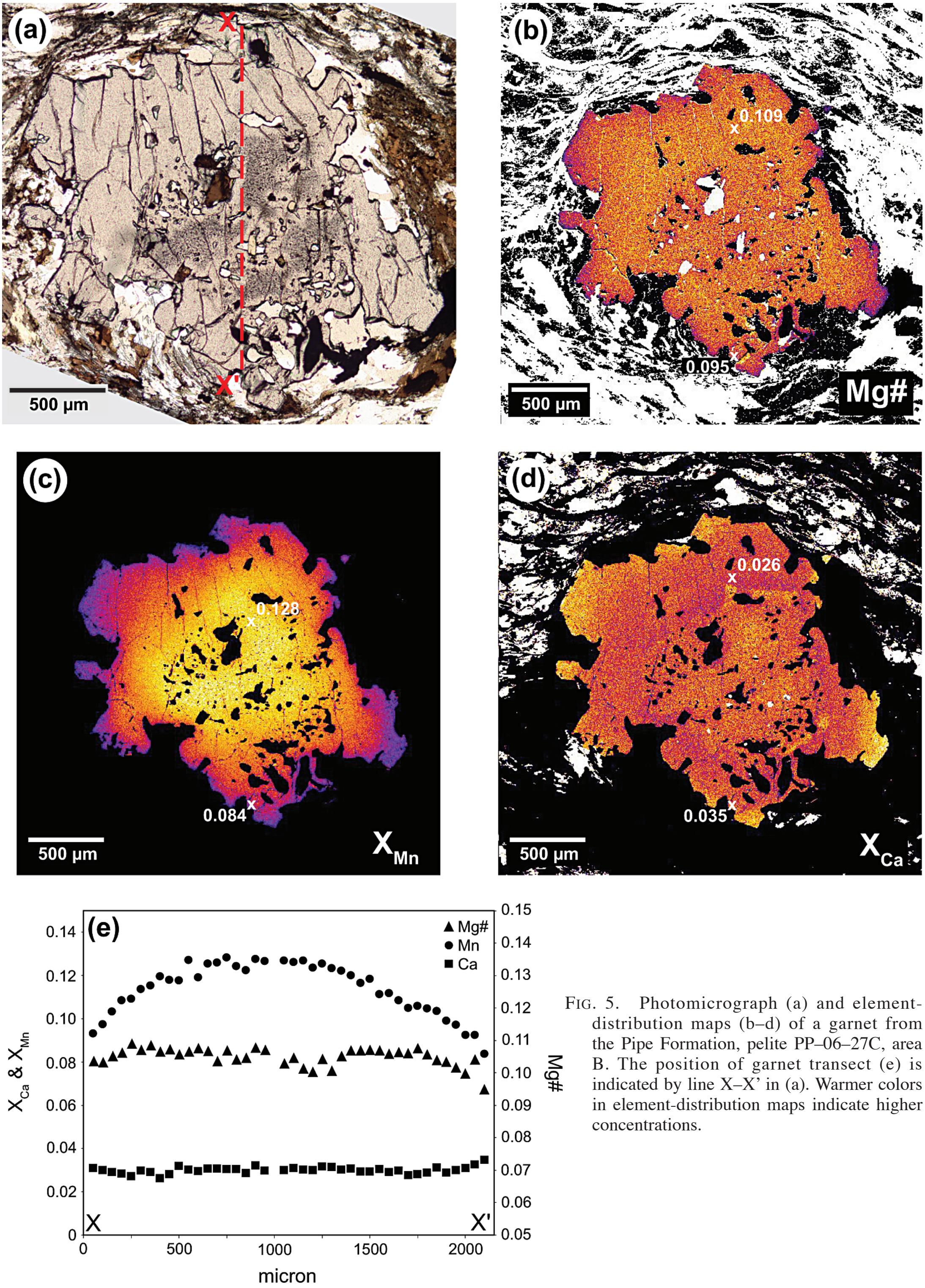

FIG. 5. Photomicrograph (a) and element-distribution maps (b–d) of a garnet from the Pipe Formation, pelite PP–06–27C, area B. The position of garnet transect (e) is indicated by line X–X’ in (a). Warmer colors in element-distribution maps indicate higher concentrations.

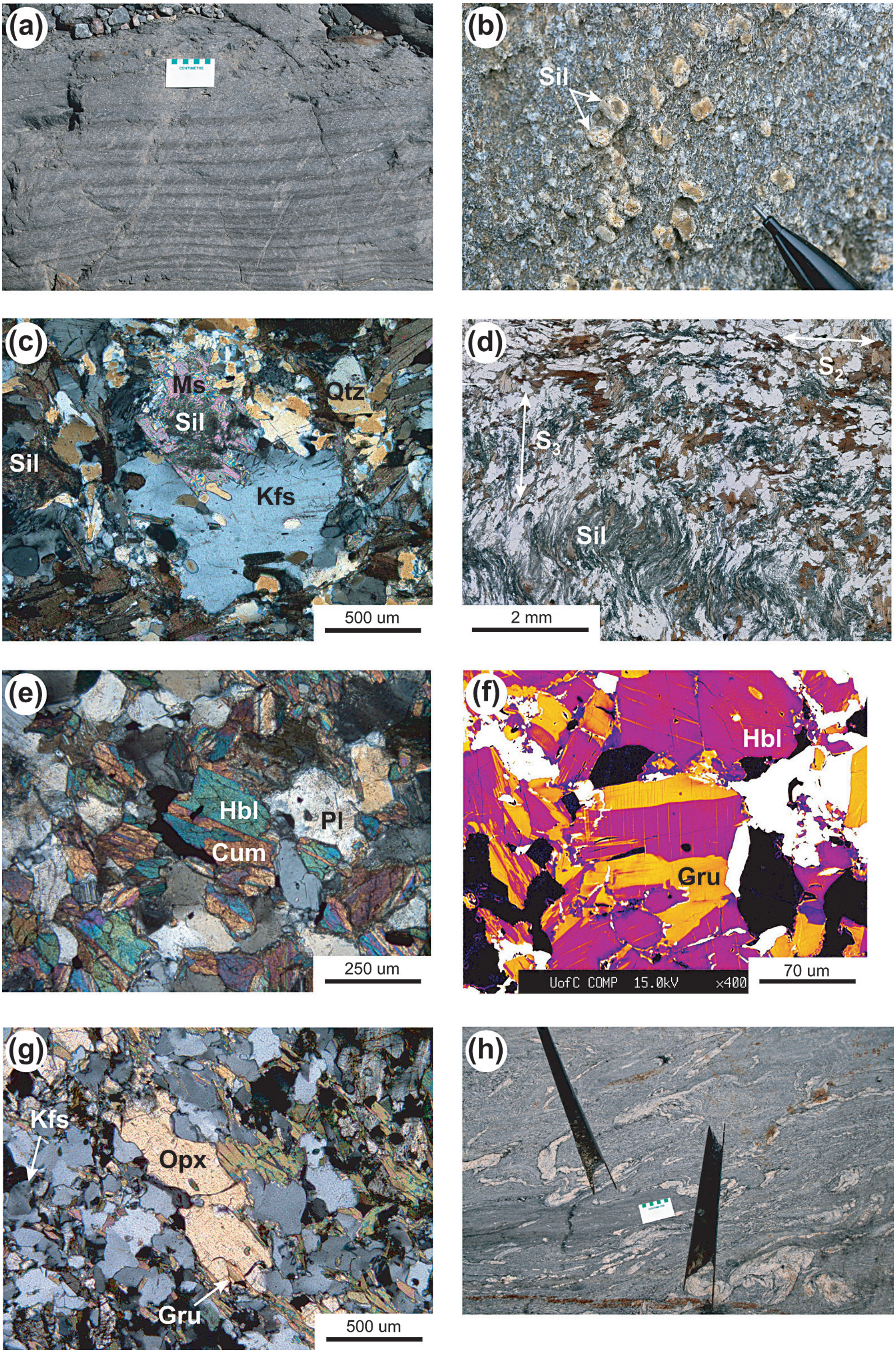
(a)
CENTIMETRE
(b)
Sil
(c)
Ms
Sil
Qtz
Sil
Kfs
500 um
(d)
S$_2$
S$_3$
Sil
2 mm
(e)
Hbl
Pl
Cum
250 um
(f)
Hbl
Gru
UofC COMP 15.0kV ×400
70 um
(g)
Kfs
Opx
Gru
500 um
(h)
CENTIMETRE

PP–06–24C is greater than that of orthopyroxene (0.14) and retrograde grunerite (0.10) (Tables 5, 6). This order of Fe–Mg fractionation is typical of coexisting grunerite and orthopyroxene in iron formations (Immega & Klein 1976, Miyano & Klein 1983).

Area E

Semipelite in the Manasan Formation from area E has the prograde metamorphic assemblage Qtz + Bt + Kfs + Sil + Pl. Although the assemblage is similar to the pelites from area C, these rocks show evidence of partial melting in the form of leucosome development (Fig. 6h). The migmatite is typically stromatic, with leucosome parallel to S_2 and folded by D_3. Contacts between the leucosome and melanosome may be sharp or diffuse over two to three centimeters. Coarse sedimentary layering can still be recognized in outcrop even though the rocks are migmatitic. Fibrous sillimanite occurs as both small lenses (<1.3 mm long) wrapped by S_2 biotite, and larger quartz–sillimanite knots (up to 2 cm long) within the melanosome. Both types of sillimanite segregation are oriented parallel to S_2. Sillimanite in the larger quartz–sillimanite knots is commonly replaced by coarse- to very coarse-grained muscovite, which is randomly oriented. The foliation of thin micaceous screens of melanosome is locally oriented parallel to S_3 in leucosome-dominated zones. Potassium feldspar is rare in the melanosome, but is a major phase along with quartz and sodic plagioclase in the leucosome. The leucosome is coarse- to very coarse-grained, with unoriented biotite and rare muscovite. Late S_3 shear bands of fine- to medium-grained biotite and muscovite locally wrap the leucosome segregations. Contacts with the leucosome are typically mylonitic, and myrmekite is common where K-feldspar contacts shear bands. Muscovite in this assemblage is interpreted to be retrograde, as it only occurs in relation to later S_3 structures. The leucosome is interpreted as *in situ* or in-source in the absence of through-going veins.

In the westernmost parts of area E, decimeter- to meter-thick migmatized horizons are interleaved with horizons of non-migmatized rock (Fig. 6h). Sillimanite is not present, and medium- to coarse-grained muscovite is intergrown with S_2 biotite. The leucosome is still dominated by igneous textures; however, anhedral biotite and locally tabular muscovite grains within the leucosome are weakly oriented parallel to S_2. Later mylonitic shear bands of very fine-grained biotite, muscovite, and quartz wrap and locally cross-cut the leucosome.

FIG. 6. Outcrop photos of pelite from the Setting Formation in area C showing: (a) primary bedding, and (b) ubiquitous knots of sillimanite giving the outcrop a speckled appearance. Scale card is in centimeters. Photomicrographs from the above pelite showing: (c) equant K-feldspar porphyroblast and fibrous sillimanite overprinted by retrograde muscovite (sample PP–08–06B), and (d) fibrous sillimanite knot flattened parallel to S_2, with fibrous sillimanite reoriented parallel to S_3 (sample PP–08–06A). (e) Photomicrograph of mafic schist from the Setting Formation in area C with single-grain intergrowths of hornblende and cummingtonite (sample PP–06–26B). (f) Back-scattered electron image of intergrown hornblende and grunerite in iron formation in the Pipe Formation in area D (sample PP–06–29C); color has been added to improve phase contrast. (g) Photomicrograph of orthopyroxene with a partial overgrowth of retrograde grunerite in iron formation from the Pipe Formation in area D (sample PP–06–29B). (h) Outcrop of migmatitic semipelite from the Manasan Formation in area E; note the locally gradational contacts of the leucosome to the right of the upper saw cut and the non-migmatite horizon present underneath the scale card.

METAMORPHIC ISOGRADS

The distinct assemblages of minerals observed in each of the six areas define several metamorphic isograds (Fig. 2). Isograd (1) occurs between area A and area B, and marks the disappearance of andalusite and staurolite from pelite assemblages. Isograd (2) occurs between area B and area D, and defines the appearance of orthopyroxene in iron formation. The dehydration of muscovite and the appearance of sillimanite plus subsolidus K-feldspar in pelite and semipelite assemblages are outlined by isograd (3) between area B and areas C and D. Sample PP–06–27A from area D contains zones with prograde muscovite and zones with sillimanite and K-feldspar, and therefore appears to be close to the isograd. In contrast to these north–northeast-trending mineral-in isograds is isograd (4), marking the approximate onset of anatectic melting between area E, and areas B and D. The "melt-in" isograd occurs at an angle to all others, and appears to cross the "sillimanite + K-feldspar-in" isograd. Further discussion of the nature of the isograds and their implications about metamorphic conditions follows the section on phase-equilibrium modeling.

PHASE-EQUILIBRIUM MODELING

Area A

The phase-diagram section for the Pipe Formation, pelite sample PP–08–08B, provides well-constrained temperature and pressure conditions for the observed assemblage Qtz + Bt + Ms + Pl + St + And + Sil + Grt (Table 1, Fig. 8a). Assuming equilibrium, the subassemblage containing And + Grt + Sil + St tightly defines P–T conditions at approximately 585°C and 3.9 kbar. However, the overprinting relationship of andalusite replacing staurolite, and sillimanite replacing both staurolite and andalusite, suggests departure from

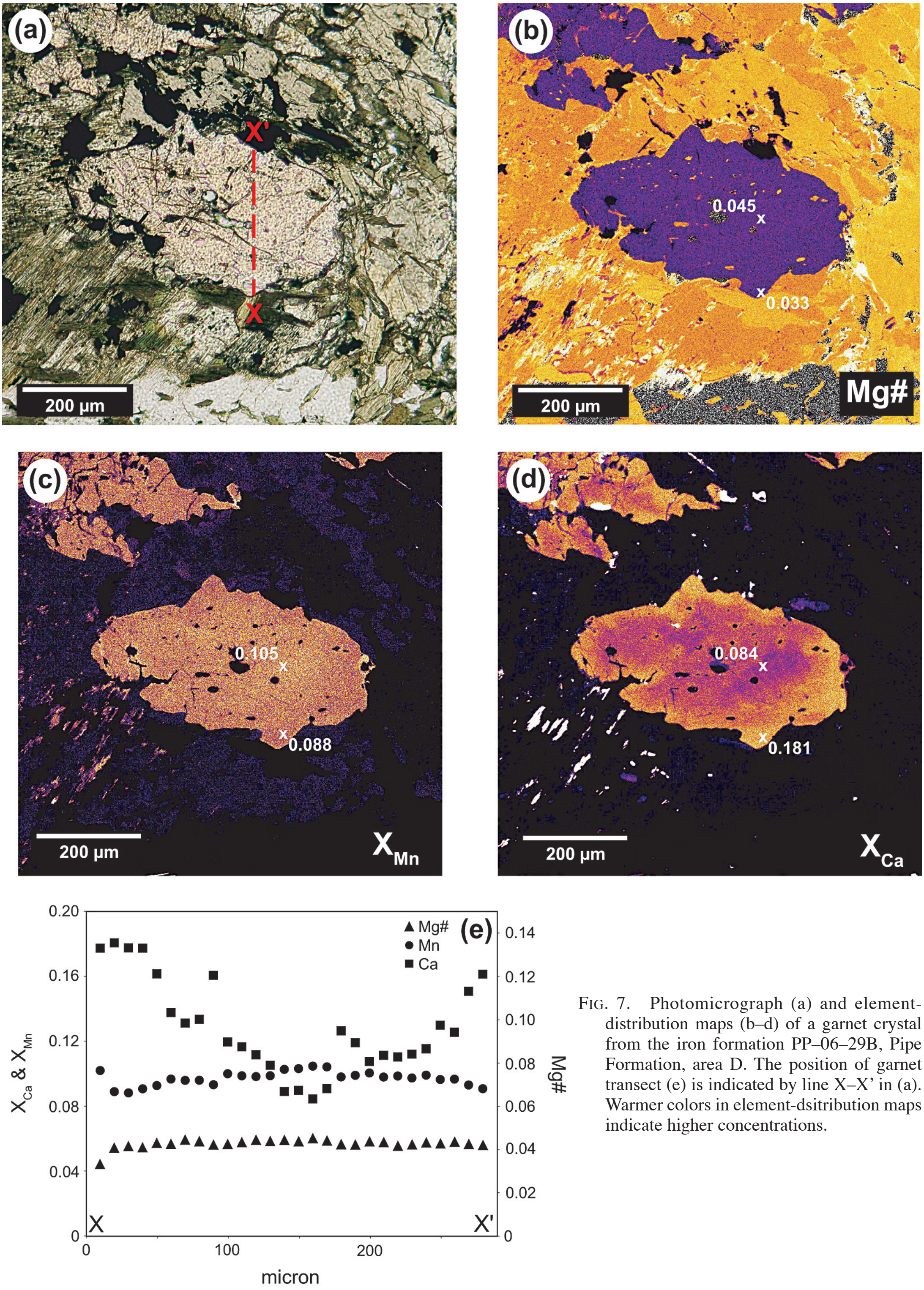

FIG. 7. Photomicrograph (a) and element-distribution maps (b–d) of a garnet crystal from the iron formation PP–06–29B, Pipe Formation, area D. The position of garnet transect (e) is indicated by line X–X' in (a). Warmer colors in element-dsitribution maps indicate higher concentrations.

equilibrium. The presence of coexisting andalusite and staurolite implies pressures less than 3.9 kbar, and the presence of sillimanite limits minimum pressures to the sillimanite field of stability. Maximum temperatures are defined by the predicted field of garnet stability; however, we note that this may not be a robust indicator of temperature. Pattison & Tinkham (2009) recognized that garnet may not dissolve during prograde metamorphism, as predicted by models based on equilibrium assemblages. Taking these limits into account, the metamorphic assemblage nevertheless defines a well-constrained P–T domain of 585–600°C and 3.7–3.9 kbar. Calculated isopleths of garnet compositions show scatter, but the centroid of the region of intersection is at a similar pressure–temperature (575°C, 4.1 kbar) as the calculated equilibrium-assemblage (Fig. 8b).

Area B

The phase-diagram section generated for the Pipe Formation, pelite sample PP–06–27C, is similar to that for PP–08–08B (Fig. 9a). The observed assemblage Bt + Qtz + Sil + Ms + Pl + Grt (Table 1) provides relatively poor constraints on pressure. The lack of andalusite and staurolite suggests higher temperatures than for area A, and if the upper-pressure limit is assumed to be the same as for sample PP–08–08B, metamorphic conditions can be estimated at 585–640°C and 3.5–3.9 kbar. Garnet isopleths show similar scatter to PP–08–08B, but the centroid of the regional intersection suggests similar pressure–temperature conditions to the modeled assemblage (590°C, 3.8 kbar, Fig. 9b).

Area C

The phase-diagram section for the Setting Formation, sample PP–06–28C, is a departure from the previous pelite sections (Fig. 10). The assemblage Qtz + Bt + Kfs + Pl + Sil with or without Grt (Table 1) and a lack of leucosome define a tightly constrained area in P–T space. The observed assemblage, minus garnet, implies metamorphic conditions of 640–660°C and 3.0–3.6 kbar. Although garnet is present in sample PP–06–28C, it occurs as isolated grains and makes up ≤1 modal % of the rock. The discrepancy between observed garnet and a predicted lack of garnet in the assemblage may be an artefact of inhomogeneous distribution of garnet within the sample used for geochemical analysis or the result of $a(H_2O) > 1$.

Three equilibrium-assemblage diagrams for the mafic schist, PP–06–26E, are shown in Figure 11. In the system NCKFMASHT, the diagram defines a fairly large field of stability for the observed assemblage Pl + Hbl + Bt + Cum (Table 1, Fig. 11a) and suggests metamorphic conditions of 540–750°C and <2–5.5 kbar. Similar results are obtained in the system MnNCKFMASHT, if Mn is not incorporated into the orthopyroxene solution (Fig. 11b). With rhodonite included as an end member in the orthopyroxene solution, the observed assemblage is not predicted anywhere in the modeled pressure and temperature interval (Fig. 11c) because of the increased field of stability of orthopyroxene.

Area D

The phase-diagram sections for the iron formation, sample PP–06–29B, are shown in Figure 12. The observed assemblage, Bt + Qtz + Gru + Opx + Mgt + Grt + Kfs + Hbl (Table 1), is not predicted in the modeled pressure–temperature space of any of the modeled systems. Fields predicted to contain the assemblage Gru + Opx + Grt + Bt + Qtz + Mgt ± Pl occur in models of the system MnNCKFMASHTO (Figs. 12b, c); however, hornblende is predicted only at lower temperatures, and K-feldspar is predicted only at higher temperatures. In Figure 12b, in which Mn is not considered in the orthopyroxene solution, this assemblage defines metamorphic conditions above the solidus, 715–735°C at 2–>7 kbar. If Mn is added as a component to the orthopyroxene solution, the same assemblage implies conditions of 580–700°C and <2–6.3 kbar, below the solidus (Fig. 12c). These differences, along with those of the mafic schist, are evaluated further in the Discussion.

Area E

Area E features the presence of leucosome in semipelite in the Manasan Formation and the initiation of anatexis. Sample PP–07–01A is leucosome-bearing and contains the prograde metamorphic assemblage Qtz + Bt + Pl + Kfs + Sil (Table 1). A phase-diagram section for this sample defines a field in P–T space of approximately 665–710°C and 3.5–5.5 kbar for this assemblage (Fig. 13).

Discussion

The melt-in isograd

The locally diffuse nature of the leucosome–melanosome contacts and the pervasive distribution of leucosome throughout the semipelite of area E argue against melt injection. Melt could have been generated as a result of an increase in temperature; however, if a temperature gradient were responsible for the overall geometry of the “melt-in” isograd, it would likely be subparallel to the other metamorphic isograds in the study area. The calculated phase-diagram sections do not suggest that semipelite of the Manasan Formation would produce anatectic melts at lower temperatures than other analyzed semipelites or metapelites. Composition, therefore, does not appear to be a factor in the initial formation of a melt.

The semipelite of the Manasan Formation at the west end of area E contains appreciable muscovite and

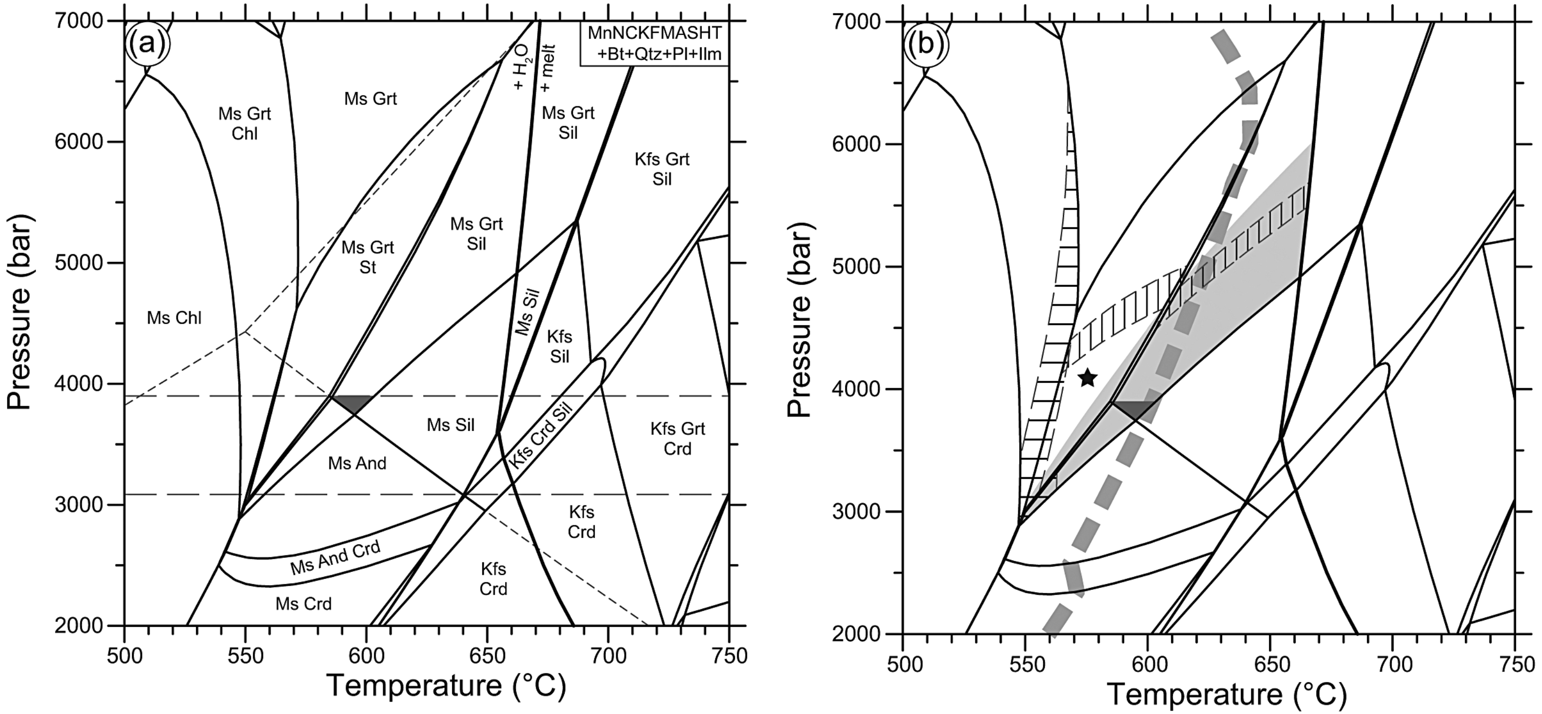

FIG. 8. (a) Equilibrium-assemblage diagram for pelite PP–08–08B from the Pipe Formation, area A. The dark grey line represents the observed metamorphic assemblage, the light grey field represents a more reasonable estimate of peak conditions of metamorphism for the assemblage (see text for details). The horizontal, long dashed grey lines indicate the pressure interval implied by pelites at the Pipe II mine. The short dashed grey lines indicate the aluminosilicate stability-fields in the system Al_2O_3–SiO_2–H_2O. (b) Calculated mineral-composition fields for garnet and plagioclase. The thick dashed line represents plagioclase of composition An_{22}. The field with vertical lines represent X_{Mn}^{Grt} of 0.066–0.086, the light grey field, X_{Ca}^{Grt} of 0.032–0.041, and horizontal lines are Mg#^{Grt} of 0.096–0.105. The black star is the approximate center of the intersecting fields of garnet composition at 575°C and 4.0 kbar.

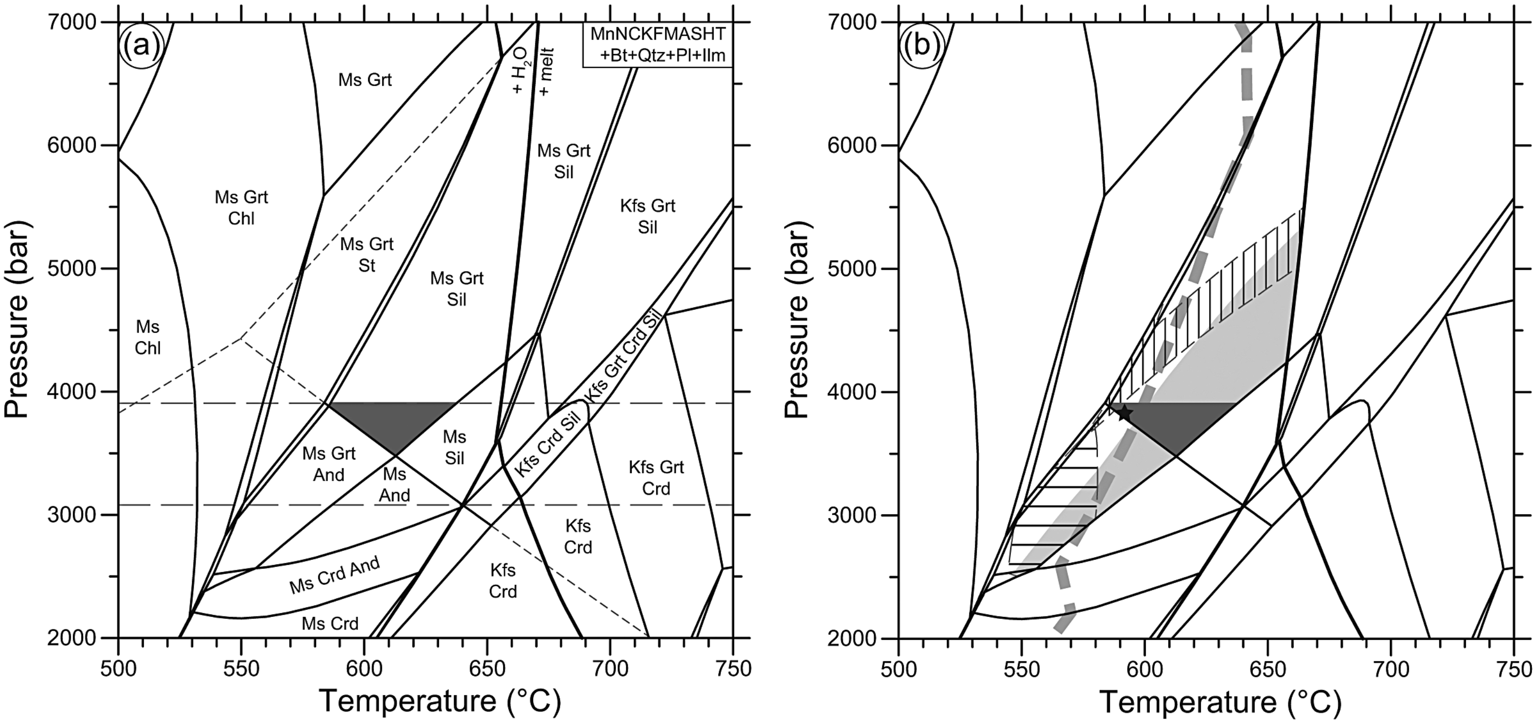

FIG. 9. (a) Equilibrium-assemblage diagram for pelite PP–06–27C, from the Pipe Formation, area B. The dark grey field represents the observed metamorphic assemblage (see text for details). The horizontal, long dashed grey lines indicate the pressure interval implied by pelites at the Pipe II mine. The short dashed grey lines indicate the aluminosilicate stability-fields in the system Al_2O_3–SiO_2–H_2O. (b) Calculated mineral-composition fields for garnet and plagioclase. The thick dashed line represents plagioclase of composition An_{22}. The field with vertical lines represent X_{Mn}^{Grt} of 0.084–0.128, the light grey field, X_{Ca}^{Grt} of 0.028–0.032, and horizontal lines are Mg#^{Grt} of 0.095–0.108. The black star is the approximate center of the intersecting fields of garnet composition at 590°C and 3.8 kbar.

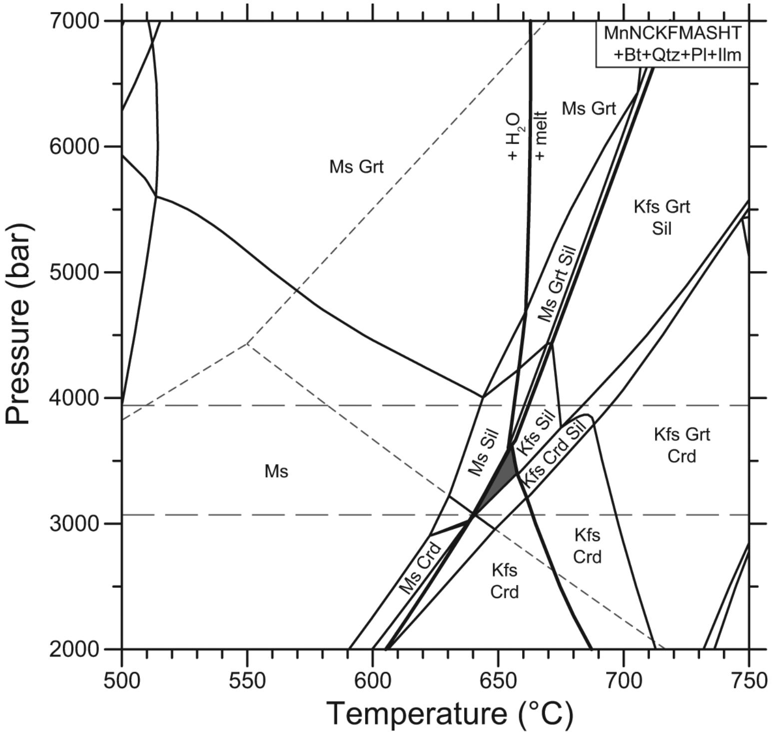

FIG. 10. Equilibrium-assemblage diagram for pelite PP–06–28C from the Setting Formation, area C. The dark grey field indicates the observed assemblage of metamorphic minerals (see text for details). The horizontal, long dashed grey lines indicate the pressure interval implied by pelites at the Pipe II mine. The short dashed grey lines indicate the aluminosilicate stability-fields in the system Al_2O_3–SiO_2–H_2O.

leucosome, but no sillimanite. These features would seem to be at odds. Dehydration of muscovite through reaction (2) is generally regarded as the onset of partial melting in semipelitic to pelitic rocks. However, partial melting may have occurred under H_2O-saturated conditions (flux-induced melting) prior to the breakdown of muscovite. The semipelites of the Manasan Formation from area B are rich in quartz, K-feldspar, and plagioclase. The addition of a H_2O-rich fluid could potentially generate significant partial melting by the reaction:

$$\text{Qtz} + \text{Kfs} + \text{Pl} + H_2O \pm \text{Ms} \pm \text{Bt} = \text{melt} \qquad (5)$$

Along the west side of area E, partial melting occurs discontinuously throughout the outcrop. Meter-scale horizons of migmatite are separated by horizons of non-migmatized semipelite. The discontinuous nature of anatexis could be caused by slight variations in composition or by fluid infiltration (White *et al.* 2005, Sawyer 2008). Localized infiltration of fluid could also explain the orientation of the "melt-in" isograd relative to the other metamorphic isograds. The growth of subsolidus K-feldspar through reaction (2) in the pelite and semipelite of areas C and D could have occurred at identical conditions of pressure and temperature as the formation of the migmatitic rocks in area E, but with a lower ambient $a(H_2O)$. The source of such a H_2O-rich fluid is problematic. Domains of granitic pegmatite several meters to tens of meters across are present in the immediate vicinity and could have introduced H_2O-rich fluids. Alternatively, fluids could have been introduced along synmetamorphic shear zones. Any shear zones, however, would have to be limited in magnitude, as no major offsets in stratigraphy are recognized.

An increasing pressure-gradient toward the south, combined with infiltrating fluids, could also be responsible for the melting of semipelites within the stability field of muscovite. St-Onge (1984) documented a muscovite–melt bathograd at similar low-pressure conditions in the Wopmay Orogen, Northwest Territories, Canada. However, pressures indicated by rocks from area C in the north and area D toward the south are in close agreement. Any pressure increase toward the south would be beyond the resolution of our methods, but it could help explain the cross-cutting orientation of the "melt-in" isograd.

The orthopyroxene-in isograd in iron formation

Comparisons of assemblages in the sillimanite-bearing pelite and grunerite-bearing iron formation at the Pipe II mine suggest that orthopyroxene first appears in iron-rich compositions at temperatures just below the sillimanite + K-feldspar isograd (roughly 620–635°C at 3–4 kbar). This is in good agreement with observations made by Immega & Klein (1976), who recognized the first occurrence of orthopyroxene in iron formations associated with muscovite-bearing, garnet–sillimanite schist heated to 600–650°C. Orthopyroxene then becomes widespread in iron formation associated with K-feldspar- and sillimanite-bearing metapelite, estimated to have reached 650–750°C and 4–6 kbar. Under both conditions, orthopyroxene was found to coexist with grunerite, but with increasing grade, the orthopy-

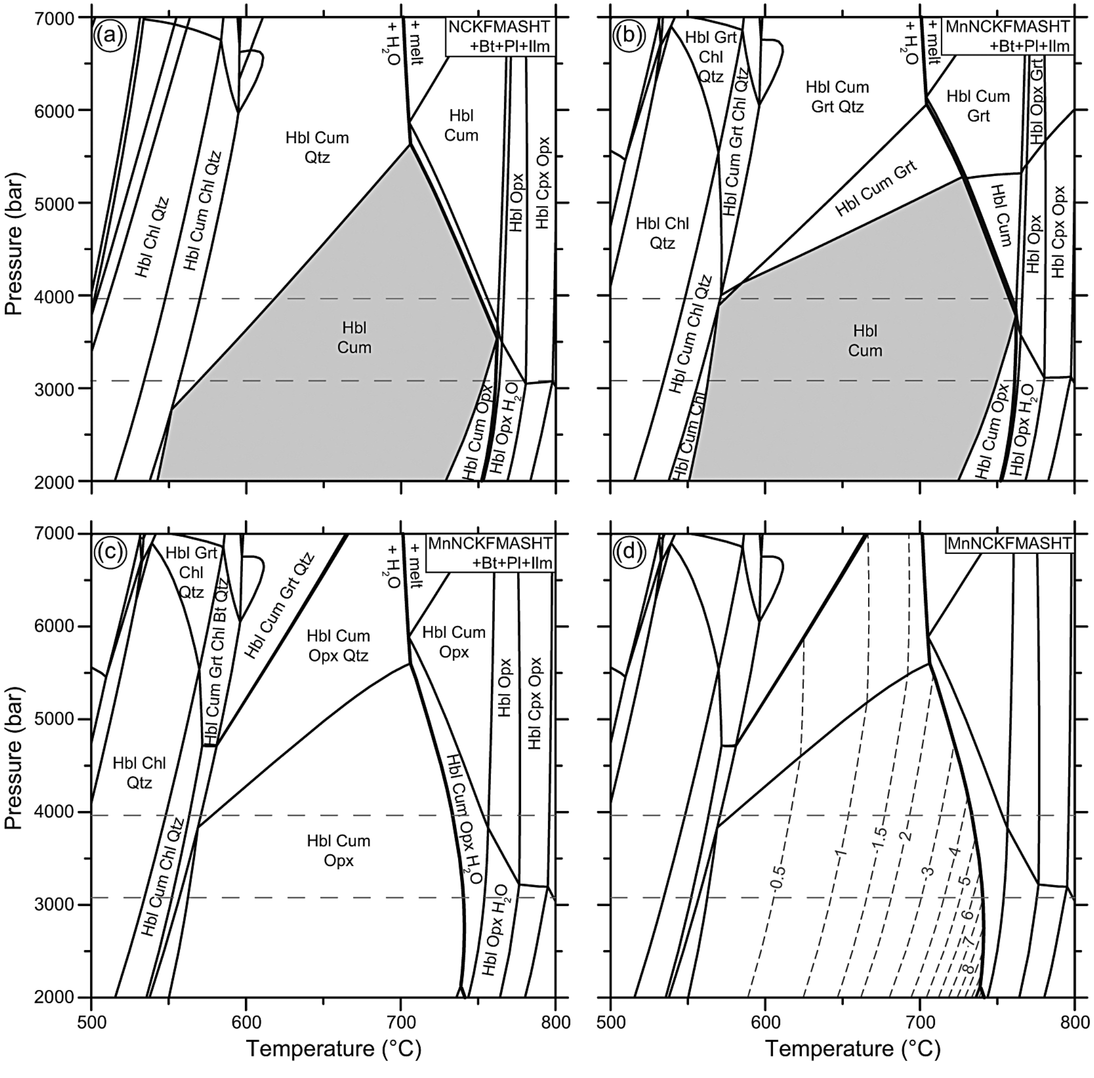

FIG. 11. Equilibrium-assemblage diagrams for mafic schist PP–06–26E from the Setting Formation, area C, in the systems (a) NCKFMASHT and (b) MnNCKFMASHT. The equilibrium-assemblage diagram in (c) was calculated with addition of rhodonite as an end member in the orthopyroxene solution. (d) Isopleths for volume % orthopyroxene, overlain on the equilibrium-assemblage diagram of (c). The grey fields in (a) and (b) represent the observed assemblages of metamorphic minerals (see text for details). The horizontal, long dashed grey lines indicate the pressure interval implied by pelites at the Pipe II mine.

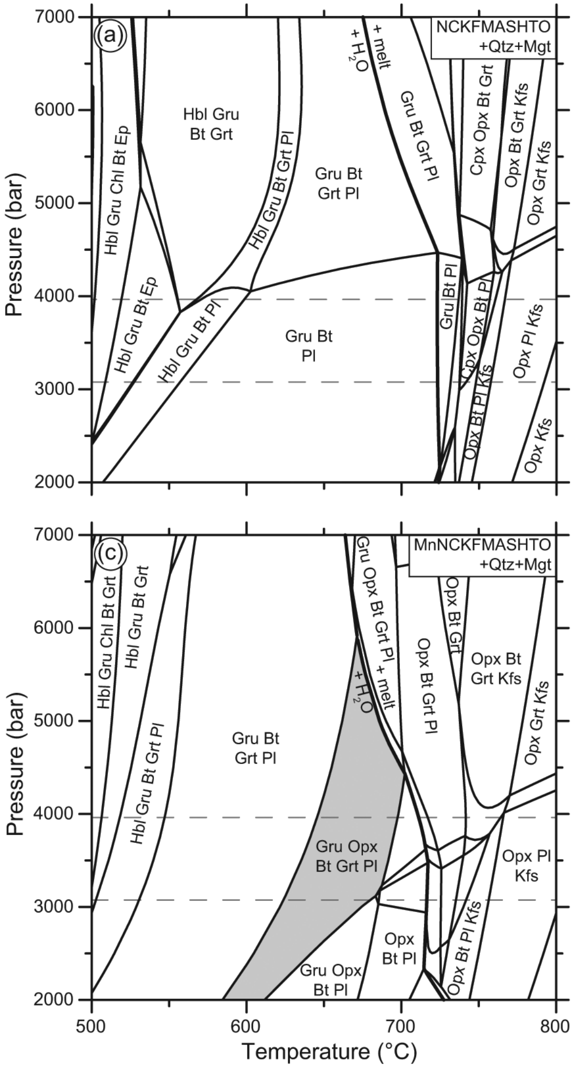

FIG. 12. Equilibrium-assemblage diagrams for iron formation PP–06–29B from the Pipe Formation, area D, in the systems (a) NCKFMASHTO and (b) MnNCKFMASHTO. The equilibrium-assemblage diagram in (c) was calculated with addition of rhodonite as an end member in the orthopyroxene solution. (d) Isopleths for volume % orthopyroxene, overlain on the equilibrium-assemblage diagram of (c). The grey fields in (b–d) represent the observed assemblages of metamorphic minerals (see text for details). The horizontal, long dashed grey lines indicate the pressure interval implied by pelites at the Pipe II mine.

roxene becomes dominant. Klein (2005) also attributed the presence of orthopyroxene to metamorphic conditions straddling the sillimanite isograd of pelitic rocks. Kahl & Schumacher (2000) identified orthopyroxene in local Mn- and Fe-rich bulk compositions in layered quartzites metamorphosed under amphibolite-facies conditions (550–640°C and 5–6.2 kbar). Bulk compositions slightly lower in Mn, or richer in Mg, were found to contain cummingtonite and hornblende in place of pyroxene. In agreement with this observation is the orthopyroxene-free mafic schist, which is considerably more magnesian and less manganiferous (Mg# 0.63, Mn# 0.0066, PP–06–26E) than the nearby orthopyroxene-bearing iron formations (Mg# 0.19, Mn# 0.0207, PP–06–29B). The temperatures implied in the formation of orthopyroxene are roughly 125°C below that of granulite-facies metamorphism as defined by the incongruent breakdown of biotite (Fig. 12, *cf.* Pattison *et al.* 2003).

The trend of the orthopyroxene-in isograd (for iron formations) in Figure 2 is indistinguishable from the subsolidus isograds found in the pelites and semipelites. This spatial relationship lends support to the proposal that the orthopyroxene-forming reaction is a thermally dependent metamorphic reaction, with little influence from changing composition of the fluid. The identification of coexisting grunerite–orthopyroxene assemblages at the Pipe II mine, as well as by Immega & Klein (1976) over a range of temperatures, suggests that the orthopyroxene-forming reaction(s) involving grunerite is likely a continuous rather than discontinuous reaction. Hollocher (1991) proposed the continuous reaction:

$$\text{Grt} + \text{Cum} + \text{Hbl} + \text{Qtz} = \text{Opx} + \text{Pl} + H_2O \quad (6)$$

for iron-rich metabasic rocks in the system Al_2O_3–FeO–MnO–Na_2O–CaO–SiO_2, which occurs around 640°C at 6 kbar. As the reaction progresses, ferromagnesian minerals would trend toward increasingly Mg-rich compositions. Although the reactants of this reaction are widespread in iron formations at the Pipe II mine, plagioclase is notably absent in orthopyroxene-bearing assemblages. The common occurrence of K-feldspar in orthopyroxene-bearing assemblages may suggest a similar type of continuous reaction involving biotite as a reactant rather than hornblende:

$$\text{Gru} + \text{Bt} + \text{Qtz} = \text{Opx} + \text{Kfs} + H_2O \quad (7)$$

however, no direct textural evidence for this reaction has been identified.

Several discrepancies between the observed assemblages in the iron formation and the modeled equilibrium assemblages were noted above. These may result from the difficulty in obtaining a representative bulk-composition in such heterogeneous rocks. Although the band chosen for bulk-rock analysis from sample PP–06–29B consists of a 2-cm-thick layer of the same mineral assemblage, the band is internally laminated, with varying proportions of its mineral constituents. The observed assemblage was not predicted in any of the modeled systems (Fig. 12). No fields with coexisting hornblende and K-feldspar are predicted; however, assemblages containing the major constituents, Bt + Qtz + Gru + Opx + Mgt + Grt (Table 1) were predicted in

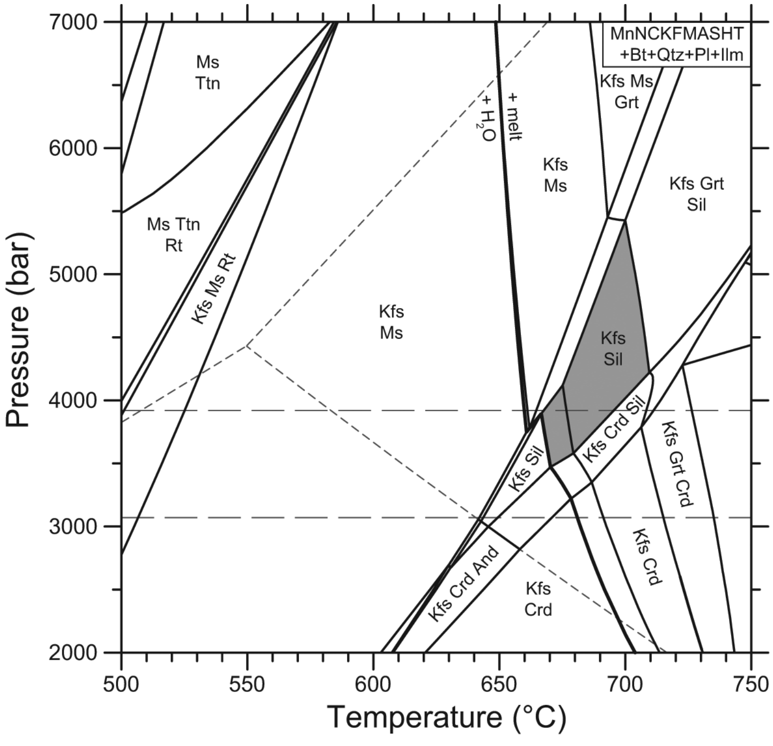

FIG. 13. Equilibrium assemblage diagram for semipelite PP–07–01A from the Manasan Formation, area D. The grey field represents the observed assemblage of metamorphic minerals (see text for details). The horizontal, long dashed grey lines indicate the pressure interval implied by pelites at the Pipe II mine. The short dashed grey lines indicate the aluminosilicate stability-fields in the system Al_2O_3–SiO_2–H_2O.

both models of the MnNCKFMASHTO system (Figs. 12b, c). In Figure 12b, assuming a pressure of 3.5 kbar, this assemblage is predicted to occur at 725°C. This is above the solidus, and significantly higher than the temperatures suggested by the position of the orthopyroxene-in isograd relative to the sillimanite + K-feldspar-in isograd in pelites (Fig. 2). With the addition of a rhodonite end-member to the orthopyroxene solution (Fig. 12c), this assemblage occurs at temperatures of 635 to 690°C. A temperature of 635°C for the initiation of orthopyroxene formation is in good agreement with placement of the metamorphic isograds (Fig. 2).

A complication in this approach arises when the rhodonite end-member is used to model the mafic schist. Without this end-member, the observed assemblage for the mafic schist is predicted over fairly large fields in Figures 11a and 11b. Equilibrium-assemblage diagrams of the host pelite in area C suggest metamorphic conditions near the middle of these fields, 640–660°C and 3–3.6 kbar. Orthopyroxene is not observed in the assemblage, and is not predicted to occur until 750°C. With the addition of rhodonite to the orthopyroxene solution in the system MnNCKFMASHT (Fig. 11c), the stability field of orthopyroxene expands to lower temperatures, 550°C. However, predicted modal amounts of orthopyroxene are very small, increasing from 0 to 1 modal % at 650°C and 3.5 kbar (Fig. 11d). At these conditions, the orthopyroxene is also predicted to be enriched in manganese, with 0.46–0.24 atoms per formula unit Mn. In the absence of garnet at low pressures, orthopyroxene is behaving as a sink for Mn, and may therefore be predicted to occur at unrealistically low temperatures. Conversely, in the garnet-bearing assemblage of PP–06–29B, orthopyroxene is predicted to appear at higher temperatures and in much greater initial volumes (Fig. 12d). Further work is needed to improve thermodynamic modeling of iron formations, and will likely require more investigations into the effects of Mn not only on orthopyroxene, but also on amphibole, magnetite, epidote, and clinopyroxene.

Interpretations about temperature, pressure and relative timing

The temperature and pressure estimates of this study are similar to those proposed by Fueten *et al.* (1986) 575–625°C and 2.5–5.75 kbar for the lower-grade assemblages observed in areas A and B, and close to the temperatures of Bleeker (1990a), 600–660°C. The best constraints on temperature and pressure at the Pipe II mine are provided by pelitic assemblages. Observed textures from samples at the Pipe II mine suggest that peak conditions of metamorphism were attained during D_2, and likely outlasted it. Local occurrences of sillimanite oriented parallel to S_3 suggest that at least middle-amphibolite-facies conditions were maintained into D_3. The orientation of the metamorphic isograds, cross-cutting the mesoscopic D_2 structures and roughly paralleling D_3 structures, imply that peak conditions of metamorphism prevailed until at least early D_3. Retrograde metamorphism became dominant during the latter stages of the D_3 event. Post-D_3 (D_4?) metamorphism comprises localized greenschist-facies assemblages along late fractures.

There is an apparent increasing thermal gradient from west to east. The lowest temperatures, 585–600°C, occur in area A, and increase to 665–700°C in the east side of area E. Given the current structural geometry, this correlates with a minimum 65°C temperature increase over roughly 420 m, perpendicular to the metamorphic isograds. Although it is possible that an igneous intrusion could be responsible for the temperature gradient, no intrusion of sufficient size to generate a thermal aureole is recognized in the Pipe II area (Macek *et al.* 2006). The age of the Molson event (*ca.* 1880 Ma) that led to the intrusion of the ultramafic sill is considered to pre-date peak metamorphism, and in addition, the intrusion is situated closest to the lowest-grade pelites. The apparent continuity of the metasedimentary sequence argues against the presence of faults with any significant displacement, as do the isobaric conditions present across the study area. Bleeker (1990a, 1990b) interpreted the andalusite as part of a retrograde mineral assemblage; however, the overprinting relationship of sillimanite and the wrapping relationship of the S_2 foliation around andalusite suggest that it is instead part of the prograde assemblage.

Recent studies suggest that staurolite and andalusite can remain as metastable phases up to 50–60°C above their predicted limits of stability (Waters & Lovegrove 2002, Pattison & Tinkham 2009). This could place temperatures in area A closer to 630°C. Although this would not explain the existence of the thermal gradient, it could reduce the apparent magnitude of the gradient to a less extreme 30°C. The thermal gradient corroborates the regional metamorphic trends with temperatures increasing eastward from this locality, possibly as high as granulite-facies grade at Paint Lake, approximately 9 km southeast across strike (Couëslan *et al.* 2007, Couëslan 2009).

An overall pressure of 3–4 kbar is considered the best estimate and is based on peak metamorphic assemblages observed from the individual areas at the Pipe II mine, with a possible increasing gradient in depth toward the south. These relatively low pressures suggest modest tectonic burial on the order of 11–14 km for this portion of the Thompson Nickel Belt. This is significantly shallower than the kyanite-generating Barrovian-style metamorphism typical of more modern continent–continent collisional zones. The results suggest that this portion of the Thompson Nickel Belt was a relatively hot and shallow zone of continental collision, compatible with interpretations in the adjacent Kisseynew Domain (Gordon 1989, White 2005), and regional interpretations of the Manitoba–Saskatchewan portion of the Trans-Hudson Orogen (Zwanzig 2004).

ACKNOWLEDGEMENTS

We thank the Manitoba Geological Survey for supporting all aspects of the field work for this study as well as providing thin sections and geochemistry. Inco Limited (now Vale Limited) allowed access and sampling at the Pipe II mine-site. Most sincere thanks to J. Macek for sharing his knowledge of the geology at the Pipe II mine and the greater Thompson Nickel Belt in general. R. Marr (UCLEMA) provided assistance on the electron microprobe. Thanks to A. Cooper and R.P. Raeside for their helpful and constructive reviews and R.F. Martin and D. Mossman for their careful editorial handling and comments.

REFERENCES

ANSDELL, K.M. (2005): Tectonic evolution of the Manitoba–Saskatchewan segment of the Paleoproterozoic Trans-Hudson Orogen, Canada. *Can. J. Earth Sci.* **42**, 741-759.

BELL, C.K. (1971): History of the Superior – Churchill boundary in Manitoba. *In* Geoscience Studies in Manitoba (A.C. Turnock, ed.). *Geol. Assoc. Can., Spec. Pap.* **9**, 5-10.

BLEEKER, W. (1990a): *Evolution of the Thompson Nickel Belt and its Nickel Deposits, Manitoba, Canada.* Ph.D. thesis, Univ. New Brunswick, Fredericton, New Brunswick.

BLEEKER, W. (1990b): Thompson area – general geology and ore deposits. *Geol. Surv. Can., Open File* **2165**, 93-125.

BLEEKER, W. & HAMILTON, M.A. (2001): New SHRIMP U–Pb ages for the Ospwagan Group: implications for the SE margin of the Trans-Hudson Orogen. *Geol. Assoc. Can. – Mineral. Assoc. Can., Program Abstr.* **26**, 15.

BOHLEN, S.R., BOETTCHER, A.L., DOLLASE, W.A. & ESSENE, E.J. (1980): The effect of manganese on olivine – quartz – orthopyroxene stability. *Earth Planet. Sci. Lett.* **47**, 11-20.

BURNHAM, O.M., HALDEN, N., LAYTON-MATTHEWS, D., LESHER, C.M., LIWANAG, J., HEAMAN, L., HULBERT, L., MACHADO, N., MICHALAK, D., PACEY, M., PECK, D.C., POTREL, A., THEYER, P., TOOPE, K. & ZWANZIG, H. (2009): CAMIRO Project 97E-02, Thompson Nickel Belt: final report March 2002, revised and updated 2003. *Manitoba Geol. Surv., Open File* **OF2008-11**.

COUËSLAN, C.G. (2009): Progress report of geological mapping at Paint Lake, Manitoba. *In* Report of Activities 2009. *Manitoba Geol. Surv.*, 108-117.

COUËSLAN, C.G., PATTISON, D.R.M. & MACEK, J.J. (2007): Hudsonian regional metamorphism in the Thompson Nickel Belt, Manitoba. *In* Report of Activities 2007. *Manitoba Geol. Surv.*, 91-97.

DE CAPITANI, C. & BROWN, T.H. (1987): The computation of chemical equilibrium in complex systems containing non-ideal solutions. *Geochim. Cosmochim. Acta* **51**, 2639-2652.

DE CAPITANI, C. & PETRAKAKIS, K. (2010): The computation of equilibrium assemblage diagrams with Theriak/Domino software. *Am. Mineral.* **95**, 1006-1016.

DIENER, J.F.A., POWELL, R., WHITE, R.W. & HOLLAND, T.J.B. (2007): A new thermodynamic model for clino- and orthoamphiboles in the system Na_2O–CaO–FeO–MgO–Al_2O_3–SiO_2–H_2O–O. *J. Metam. Geol.* **25**, 631-656.

DROOP, G.T.R. (1987): A general equation for estimating Fe^{3+} concentrations in ferromagnesian silicates and oxides from microprobe analyses, using stoichiometric criteria. *Mineral. Mag.* **51**, 431-435.

FUETEN, F. & ROBIN, P.-Y.F. (1989): Structural petrology along a transect across the Thompson Belt, Manitoba: dip slip at the western Churchill–Superior boundary. *Can. J. Earth Sci.* **26**, 1976-1989.

FUETEN, F., ROBIN, P.-Y.F. & PICKERING, M.E. (1986): Deformation in the Thompson Belt, central Manitoba: a progress report. *Geol. Surv. Can., Current Res.* **86-1B**, 797-809.

GAPAIS, D., POTREL, A., MACHADO, N. & HALLOT, E. (2005): Kinematics of long-lasting Paleoproterozoic transpression within the Thompson Nickel Belt, Manitoba, Canada. *Tectonics* **24**, TC3002, doi: 10.1029/2004TC001700.

GORDON, T.M. (1989): Thermal evolution of the Kisseynew sedimentary gneiss belt, Manitoba: metamorphism at an early Proterozoic accretionary margin. *In* Evolution of Metamorphic Belts (J.S. Daly, R.A. Cliff & B.W.D. Yardley, eds.). *Geol. Soc., Spec. Publ.* **43**, 233-243.

GRAPHCHIKOV, A.A. (1992): Orthopyroxene – magnetite – quartz oxygen barometer for Mn-bearing rocks (experimental calibration). *Proc. Indian Acad. Sci., Earth and Planet. Sci.* **101**, 191-199.

GREEN, E., HOLLAND, T. & POWELL, R. (2007): An order-disorder model for omphacitic pyroxenes in the system jadeite – diopside – hedenbergite – acmite, with applications to eclogitic rocks. *Am. Mineral.* **92**, 1181-1189.

HEAMAN, L.M., PECK, D. & TOOPE, K. (2009): Timing and geochemistry of 1.88 Ga Molson igneous events, Manitoba: insights into the formation of a craton-scale magmatic and metallogenic province. *Precamb. Res.* **172**, 143-162.

HOLLAND, T.J.B. & POWELL, R. (1998): An internally-consistent thermodynamic dataset for phases of petrological interest. *J. Metam. Geol.* **16**, 309-344.

HOLLOCHER, K. (1991): Prograde amphibole dehydration reactions during high-grade regional metamorphism, central Massachusetts, U.S.A. *Am. Mineral.* **76**, 956-970.

IMMEGA, I.P. & KLEIN, C. (1976): Mineralogy and petrology of some metamorphic Precambrian iron-formations in southwestern Montana. *Am. Mineral.* **61**, 1117-1144.

KAHL, W.-A. & SCHUMACHER, J.C. (2000): Multiple pyroxene and amphibole assemblages in the amphibolite facies: bulk compositional controls. *Am. Mineral.* **85**, 1606-1616.

KLEIN, C. (1966): Mineralogy and petrology of the metamorphosed Wabush iron formation, southwestern Labrador. *J. Petrol.* **7**, 246-305.

KLEIN, C. (2005): Some Precambrian banded iron-formations (BIFs) from around the world: their age, geologic setting, mineralogy, metamorphism, geochemistry, and origin. *Am. Mineral.* **90**, 1473-1499.

KROGH, E.J. (1977): Origin and metamorphism of iron formations and associated rocks, Lofoten-Vesterålen, N. Norway. I. The Vestpolltind Fe–Mn deposit. *Lithos* **10**, 243-255.

MACEK, J.J., ZWANZIG, H.V. & PACEY, J.M. (2006): Thompson Nickel Belt geological compilation map, Manitoba. *Manitoba Geol. Surv., Open File Rep.* **OF2006-33**.

MIYANO, T. & KLEIN, C. (1983): Phase relations of orthopyroxene, olivine, and grunerite in high-grade metamorphic iron-formation. *Am. Mineral.* **68**, 699-716.

MORIMOTO, N. (1989): Nomenclature of pyroxenes. *Can. Mineral.* **27**, 143-156.

PAKTUNÇ, A.D. & BAER, A.J. (1986): Geothermobarometry of the northwestern margin of the Superior Province: implications for its tectonic evolution. *J. Geol.* **94**, 381-394.

PATTISON, D.R.M., CHACKO, T., FARQUHAR, J. & MCFARLANE, C.R.M. (2003): Temperatures of granulite-facies metamorphism: constraints from experimental phase equilibria and thermobarometry corrected for retrograde exchange. *J. Petrol.* **44**, 867-900.

PATTISON, D.R.M. & TINKHAM, D.K. (2009): Interplay between equilibrium and kinetics in prograde metamorphism of pelites: an example from the Nelson aureole, British Columbia. *J. Metam. Geol.* **27**, 249-279.

PETERSEN, E.U., ANOVITZ, L.M. & ESSENE, E.J. (1984): Donpeacorite, (Mn,Mg)$MgSi_2O_6$, a new orthopyroxene and its proposed phase relations in the system $MnSiO_3$–$MgSiO_3$–$FeSiO_3$. *Am. Mineral.* **69**, 472-480.

POWELL, R. & HOLLAND, T. (1999): Relating formulations of the thermodynamics of mineral solid solutions: activity modelling of pyroxenes, amphiboles, and micas. *Am. Mineral.* **84**, 1-14.

SAWYER, E.W. (2008): *Atlas of Migmatites*. The Canadian Mineralogist, Spec. Publ. **9**, NRC Research Press, Ottawa, Ontario.

SAWYER, E.W. & ROBIN, P.-Y.F. (1986): The subsolidus segregation of layer-parallel quartz–feldspar veins in greenschist to upper amphibolite facies metasediments. *J. Metam. Geol.* **4**, 237-260.

SCOATES, J.S., WALL, C.J., FRIEDMAN, R.M., BOOTH, K., SCOATES, R.F.J., COUËSLAN, C. & MACEK, J. (2010): Recent progress in determining the precise age of ultramafic sills and mafic dikes associated with mineralization in the Thompson Nickel Belt, Manitoba, Canada. *In* 11th Int. Platinum Symp. (Sudbury), Abstr. Vol. (G.H. Brown, P.J. Jugo, C.M. Lesher, & J.E. Mungall, eds.). *Ontario Geol. Surv., Misc. Release–Data* **269**.

SCOATES, R.F.J., MACEK, J.J. & RUSSELL, J.K. (1977): Thompson Nickel Belt Project. *In* Report of Field Activities 1977. *Manitoba Mineral Resources Division*, 47-53.

SPEAR, F.S. (1993): *Metamorphic Phase-Equilibria and Pressure – Temperature – Time Paths*. Mineralogical Society of America, Washington, D.C.

ST-ONGE, M.R. (1984): The muscovite–melt bathograd and low-P isograd suites in north-central Wopmay Orogen, Northwest Territories, Canada. *J. Metam. Geol.* **2**, 315-326.

STIMPFL, M. (2005): The Mn, Mg-intracrystalline exchange reaction in donpeacorite ($Mn_{0.54}Ca_{0.03}Mg_{1.43}Si_2O_6$) and its relation to the fractionation behavior of Mn in Fe, Mg-orthopyroxene. *Am. Mineral.* **90**, 155-161.

STÖCKHERT, B., BRIX, M.R., KLEINSCHRODT, R., HURFORD, A.J. & WIRTH, R. (1999): Thermochronology and microstructures of quartz – a comparison with experimental flow laws and predictions on the temperature of the brittle–plastic transition. *J. Struct. Geol.* **21**, 351-369.

TINKHAM, D.K. & GHENT, E.D. (2005): Estimating P–T conditions of garnet growth with isochemical phase diagram sections and the problem of effective bulk-composition. *Can. Mineral.* **43**, 35-50.

WATERS, D.J. & LOVEGROVE, D.P. (2002): Assessing the extent of disequilibrium and overstepping of prograde metamorphic reactions in metapelites from the Bushveld Complex aureole, South Africa. *J. Metam. Geol.* **20**, 135-149.

WEBER, W. (1990): The Churchill–Superior Boundary Zone, southeast margin of the Trans-Hudson orogen: a review. *In* The Early Proterozoic Trans-Hudson Orogen of North America (J.F. Lewry & M.R. Stauffer, eds.). *Geol. Assoc. Can., Spec. Pap.* **37**, 41-55.

WHITE, D.J. (2005): High-temperature, low-pressure metamorphism in the Kisseynew domain, Trans-Hudson orogen: crustal anatexis due to tectonic thickening? *Can. J. Earth Sci.* **42**, 707-721.

WHITE, R.W., POMROY, N.E. & POWELL, R. (2005): An *in situ* metatexite–diatexite transition in upper amphibolite facies rocks from Broken Hill, Australia. *J. Metam. Geol.* **23**, 579-602.

WHITE, R.W., POWELL, R. & HOLLAND, T.J.B. (2001): Calculation of partial melting equilibria in the system Na_2O–CaO–K_2O–FeO–MgO–Al_2O_3–SiO_2–H_2O (NCKFMASH). *J. Metam. Geol.* **19**, 139-153.

WHITE, R.W., POWELL, R. & HOLLAND, T.J.B. (2007): Progress relating to calculation of partial melting equilibria for metapelites. *J. Metam. Geol.* **25**, 511-527.

WHITE, R.W., POWELL, R., HOLLAND, T.J.B. & WORLEY, B.A. (2000): The effect of TiO_2 and Fe_2O_3 on metapelitic assemblages at greenschist and amphibolite facies conditions: mineral equilibria calculations in the system K_2O–FeO–MgO–Al_2O_3–SiO_2–H_2O–TiO_2–Fe_2O_3. *J. Metam. Geol.* **18**, 497-511.

ZWANZIG, H.V. (1998): Structural mapping of the Setting Lake area. *In* Report of Activities 1998. *Manitoba Geol. Surv.*, 40-45.

ZWANZIG, H.V. (2004): Hot, thin and mineral-rich – evolution of the Paleoproterozoic Trans-Hudson Orogen in western Canada. *In* Report of Activities 2004. *Manitoba Geol. Surv.*, iv-v.

ZWANZIG, H.V., MACEK, J.J. & MCGREGOR, C.R. (2007): Lithostratigraphy and geochemistry of the high-grade metasedimentary rocks in the Thompson Nickel Belt and adjacent Kisseynew Domain, Manitoba: implications for nickel exploration. *Econ. Geol.* **102**, 1197-1216.

Received September 28, 2010, revised manuscript accepted June 4, 2011.